UNIVERSITÀ DEGLI STUDI DI PADOVA

Dipartimento di Fisica e Astronomia "Galileo Galilei"

Corso di Laurea in Fisica

Tesi di Laurea

First plasma operations of the SPIDER experiment

Relatore

Dr. Gianluigi Serianni

Correlatore

Dr. Emanuele Sartori

Laureando

Letizia Ferbel

Anno Accademico 2017/2018

Abstract

SPIDER experiment, hosted at Consorzio RFX in Padova, is one of the most important contribution of study for ITER. SPIDER (Source for Production of Ion of Deuterium Extracted from RF plasma) is the first experiment device built and operating, aiming and testing the extraction of negative ion beam from an ITER size ion source and it is also one of the most important experiment on nuclear fusion currently underway.
The first operations of SPIDER concerned the analysis and study of the system to reach the plasma ignition. There have been conducted separate studies on the Gas Injection and Vacuum System (GVS), on the Tungsten filaments feeding the vacuum vessel with free electrons and on the Radio Frequency which transfer power and ionize the gas coming from the GVS.
The three studies made finally possible to achieve the 6th June the first SPIDER plasma ignition. From this moment on, the main goal became the study of the characteristic of the generated plasma and the research of the optimal combination of the controllable parameters to ignite a plasma that could also sustain itself as long as possible.
The experimental studies were constantly accompanied by the development of a model in order to provide a simulation and previsions of the system behavior.

Sommario

L'esperimento SPIDER, costruito presso il Consorzio RFX di Padova, é uno dei contributi di ricerca più importanti per ITER. SPIDER (Sorgente per la produzione di Ioni di Deuterio estratti da un plasma di RadioFrequenza) é il primo dispositivo di ricerca costruito e operativo che mira a e testa l'estrazione di un fascio di ioni negativi da una sorgente di ioni delle dimensioni di ITER; inoltre é uno dei più importanti esperimenti di fusione nucleare attualmente in opera.
Le prime operazioni di SPIDER erano atte all'analisi e studio del sistema in modo da poter raggiungere l'accensione del plasma. Sono stati condotti degli studi separati sul sistema di iniezione gas e il sistema da vuoto (GVS); sui filamenti di tungsteno, che forniscono elettroni liberi nella camera da vuoto; sulla Radio Frequenza che trasferisce potenza e ionizza il gas fornito dal GVS.
I tre studi hanno permesso di raggiungere il 6 Giugno la prima accensione di plasma in SPIDER. Da questo momento in poi, lo scopo é diventato lo studio delle caratteristiche del plasma generato e la ricerca della combinazione ottimale dei parametri controllabili risultanti nell'accensione di un plasma che potesse anche autosostenersi.
Le sessioni sperimentali sono state accompagnate dallo sviluppo di codici e modelli in grado di simulare e prevedere la risposta del sistema.

Contents

Chapter 1

Introduction

ITER is an international nuclear fusion research and engineering project built in Cadarache, France. The idea was born in 1985, nearly 30 years ago, by the collaboration of the European Union, India, Japan, South Korea, the Soviet Union and the USA with the intent to develop a new, cleaner and more sustainable source of energy. At the moment is one of the most ambitious energy project in the world.
One of the most important contributions of Italy come from the ITER Neutral Beam Test Facility (PRIMA) built at Consorzio RFX in Padova. PRIMA includes a full size ion source with low voltage extraction called SPIDER and a full size neutral beam injector at full beam power called MITICA. SPIDER is the fist experiment device built and operating, aiming at testing the extraction of negative ion beam (made of H^- ions in the first stages and D^- ions in the later ones) from an ITER size ion source.
The main purpose of the SPIDER (Source for Production of Ion of Deuterium Extracted from RF plasma) experiment is to optimize the performance of an ITER-like ion source by maximizing the extracted negative ion current density and its spatial uniformity and by minimizing the ratio of co-extracted electrons, in order to match the ITER requirements.

1.1 SPIDER design and description

The beam source for SPIDER (Source for Production of Ion of Deuterium Extracted from Rf plasma) foresees the same plasma source as for ITER and the same first two grids (plasma and extraction grids), that extract the negative ions from the plasma source, by applying a voltage up to 12 kV. In SPIDER there is just another acceleration stage of 100 kV to the grounded grid. The beam source for SPIDER consists of a complex chamber (plasma source) where the gas is injected and ionized in order to produce negative ions and a system of grids at different potential (extractor and accelerator) that extracts and accelerates the ions out of the source. The two subsystems are fixed to the common support structure that features the mechanical interface towards the vacuum vessel where the source operate.

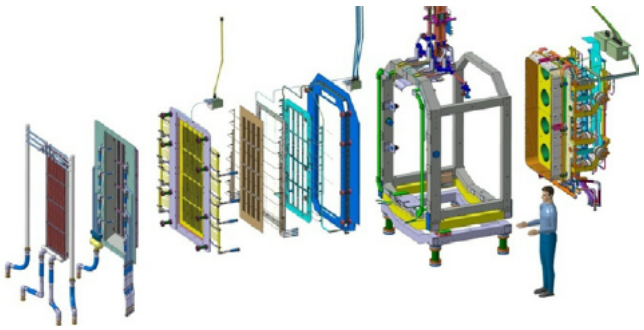

Figure 1.1: Schematic view of SPIDER

The RF ion source is the component where the negative ions are generated. The RF ion source features amain space, enclosed in a structure called source case and facing the plasma grid, on whose surface most of negative ions are generated, and eight rear smaller chambers called drivers, where the gas is injected (hydrogen or deuterium). The drivers (1.2) are the components where the power is transferred in the RF ion source and the plasma is generated. They are cylindrical structures directly connected with the source case. The Faraday shield (FS) is a cylindrical cup that protects the driver case from the plasma.

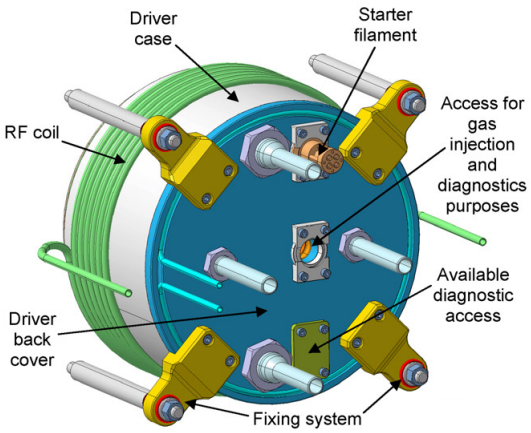

Figure 1.2: Driver assembly, overall view

RF coils are wound around the lateral wall of the drivers, and connected to a 1 MHz oscillator, transfer the RF power and ionize the gas: the resulting plasma flows then into the main chamber.
The RF ion source also includes a series of auxiliary systems: the electric circuit for power input, the cooling circuits for heated components, the gas supply system, three ovens to dispense the caesium inside the source, starter filaments to initiate the plasma and several diagnostic sensors to monitor and control the source behavior.

A dedicated extraction/acceleration system has been designed for the SPIDER experiment (1.1), made of three grids the plasma grid (PG), the extraction grid (EG) and the grounded grid (GG) plus a bias plate (BP). Each grid features 1280 apertures, where the ion beamlets are extracted from the ion source and accelerated up to 100 kV.

1.2 First operations

SPIDER's first experimental campaign began around May 2018. First operation has been based on the study of the experiment and its behavior under stresses. In the first few weeks the campaign was centered on the individual studies of gas system, filaments and RF power supply.Afterwards the main focus has become the Plasma injection and the discovery of the best combination of the three parameters above mentioned.

Chapter 2

Gas

2.1 General Description

The first part of characterization of the SPIDER experiment has been focused on the Gas Injection and Vacuum System (GVS): with the goal to confirm, some expected values and relationships, and test the instruments involved and the experiment in general. The GVS can be split in the following main items:

- Vacuum System
- Gas injection
- Measuring System
- Control System

The SPIDER vacuum Vessel is a cylindrical chamber made in stainless steel, which size is around 100 m^3. The injection system should provide H_2 gas (in first operations and D_2 gas in the later ones, like is gonna be in ITER) in order to achieve and test the system for a maximum flow rate of 5 Pa·m^3/s (and 3.5 Pa·m^3/s respectively for Deuterium) and supply gas for the beam source for at least 3600 s as required for ITER. The vacuum system provide a working pressure of 0.3 Pa inside the beam source and a pressure lower than 0.05 Pa outside the source. The vacuum system also allows to evacuate the vessel and to regenerate the cyopumps after the experimental sessions.

2.1.1 Vacuum system

The vacuum system is composed in forevacuum and high-vacuum stages. The high vacuum stage comprises 4 turbomolecular pumps, in order to establish the working pressure inside the vessel during the experiments, and 8 cryopumps, with the porpuse of establishing the crossover pressure and during the regeneration stage. It also includes 4 full range pressure gauges and 4 capacitive gauges connected directly with the vessel. In particular, the capacitive sensors are absolute pressure gauge, used to measure the pressure in vessel and in the ion-source during the operations.

2.1.2 Gas injection

The beam source for SPIDER consist of a complex chamber (plasma source) where the gas is injected and ionized in order to produce negative ions, and a system of grids at different potential (used to accelerate or deviate particles) by which the ions are extracted from the source and accelerated.
The gas injection system must inject a controlled gas flow into the plasma source, following a sequence set up by the experiment control system. The gas that can be injected is:

- Hydrogen or deuterium as process gas

- Helium, Argon and Neon as impurity gas
- Nitrogen as a service gas and for venting the SPIDER vessel

The gas injection system is divided into two similar sub-units: the first dedicated to Hydrogen or Deuterium and the second one to provide redundancy in case of failure or maintenance of the first sub-unit, or to inject impurity gas into the beam source or in the vessel. The gas pipes are routed from the gas injection system to the vessel with a bushing located in the bottom part of the vessel. The gas is supplied to the beam source trough a dedicated feed system made of hydraulic pipes as shown in the following figure 2.1.

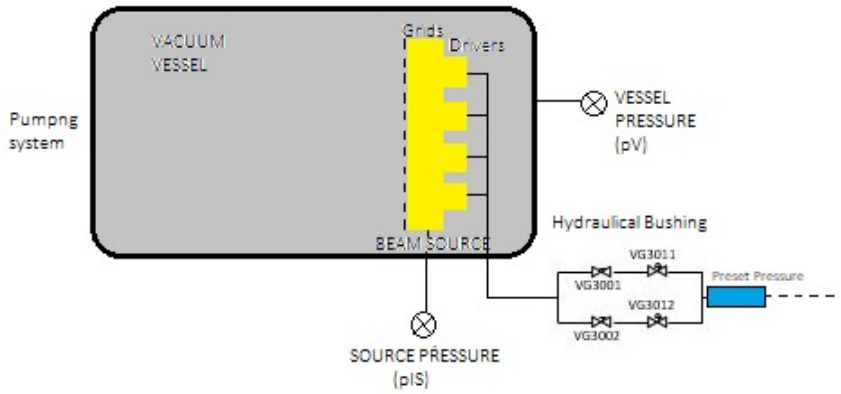

Figure 2.1: Pipeline Schematic

As it is possible to see there are two sub-lines connected to two pneumatic valves names which switch ON of the gas flow in the respective line and set the working pressure. Right after, there are VG001 and VG002: two micro-metric valves which set the injected gas flux in the system. The two micrometric valves present the possibility to change the cross sectional area of flow constriction by using a graduated scale witch is possible to completely turn 6 times and it present 0.01 mm ticks corresponding to $1/25$ turn.
The two pipelines connect the gas source to the vessel by firstly injecting the same quantity of gas in the eight drivers.
The absolute capacitive pressure gauges, at least for the first operation where placed inside the vessel and at the end of the measure pipeline.

Operating conditions
It is required that the gas injection system work in continuous regime up to 3600 s. The required filling pressure in the chamber during the operations is 0.3 *Pa*.
The gas injection system must supply a beam source with Hydrogen at a flow rate of 5 Pa·m^3/s (or Deuterium at 3.5 Pa·m^3/s, moreover, it must give the possibility to measure the total amount of injected gas during the operations in order to evaluate the load to the cryopumps.

2.2 Experimental characterization and setup

The preliminary test had been checking the good conditions, the cleanliness of the pipes, the cryopums and the vacuum sealing with leak test, vacuum tests, flow tests and so on.
After that the Experimental characterization began. The aim of Experimental characterization was to verify the requirements and find relationships and correlations between the inlet and outgoing gas passing through the experiment, check the requirement of the experiment expressed in the previous section. In addition, to verify the applicability of the ELISE experiment requirement for gas in order to ignite plasma in the SPIDER experiment.
The ELISE (Extraction from a Large Ion Source Experiment) test rig constitutes a source half as large as that for ITER later. This experiment results on plasma ignition permitted to devise a range of working pressure and

gas puffs to investigate in the SPIDER. The NBI ITER requirement were a pressure in the ion-source of 0.3 Pa with a gas puffing at the moment of the switch on of RF power and the use of inital filaments providing at least 2 mA of electron current, the request for the ignition has been confirmed by ELISE.

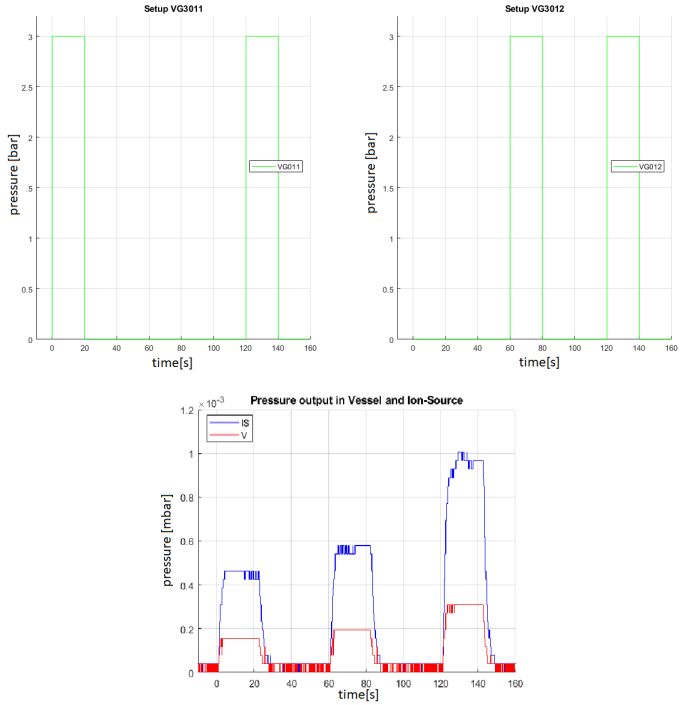

Figure 2.2: Example of a Shot of preliminary operations

The figure 2.2 show an example of the setup of the mechanic valves and so that, the wave form of the inlet, upstream pressure and the output measured in Vessel and at the Ion-source.
In the setup operation it is possible to choose the value of the upstream pressure arriving at the mechanical valves and the wave form of the gas during the time of the operation. It is also possible to choose the aperture of the micrometric valves VG3011 and VG3012, so that the gas flow in the line and their interference.
What needed to be studied was the response to the gas injection from the mechanical valves to the output, the gas flow coming out of the micrometric valves at different apertures.
In this phase of the characterization of the system there where two capacitive absolute gauges: one in the vacuum Vessel and one at the output of the measure-line, Ion-Source. The presence of both these two instruments permitted to find relationships and correlations between the pressures in those two different points. In the following operation there was just the capacitive gauge in the Ion-Source and so, one less instrument to study the system.

2.3 Piping analysis with LTSPICE

A gas flow exhibits different regime when flowing in the considered system. In the case of SPIDER the flow regimes that can be found are the following:

- *Laminar flow*, characteristic of the injection pipeline.
- *Molecular flow*, characteristic of the measure pipeline.
- *Chocked flow*, is the regime used to describe what happens in the micrometric valves (i.e valves with a variable orifice surface) and also the flow describing the pipeline's outlet into the drivers volume.

Laminar flow. In laminar flow, sometimes called streamline flow, the velocity, pressure, and other flow properties at each point in the fluid remain constant. Laminar flow over a horizontal surface may be thought of as consisting of thin layers, or laminae, all parallel to each other. The fluid in contact with the horizontal surface is stationary, but all the other layers slide over each other. Laminar flow in a straight pipe can be considered as the relative motion of a set of concentric cylinders of fluid, the outside one fixed at the pipe wall and the others moving at increasing speeds as the center of the pipe is approached. Laminar flow is common only in cases in which the flow channel is relatively small, the fluid is moving slowly, and its viscosity is relatively high.
Molecular flow. In molecular flow regime gas molecule-surface interaction are the governing phenomena. This flow is based on some basic assumptions: 1. the incident molecule-surface collisions are much more numerous than incident molecule-incident molecule collision; 2. incident molecule-surface collisions are much more numerous than incident molecule-reflected molecule collisions, i.e. the incident flow is undisturbed by the presence of the body and the equilibrium velocity distribution of the incident molecules is changed only by collision with the body; 3. the molecules follow the Maxwell-Boltzmann distribution. Since there is no interaction between the molecules it is possible to compute separately the effect on the surface of the incident and reflected molecules.
Chocked flow. Choked flow is a fluid dynamic condition associated with the Venturi effect. When a flowing fluid at a given pressure and temperature passes through a restriction (such as the throat of a convergent-divergent nozzle, orifices or a valve in a pipe) into a lower pressure environment the fluid velocity increases. At initially subsonic upstream conditions, the conservation of mass principle requires the fluid velocity to increase as it flows through the smaller cross-sectional area of the restriction. At the same time, the Venturi effect causes the static pressure, and therefore the density, to decrease downstream beyond the restriction. Choked flow is a limiting condition where the mass flow will not increase with a further decrease in the downstream pressure environment while upstream pressure is fixed. Is important to underline that the limited parameter is velocity, and thus mass flow can be increased with increased upstream pressure (increased fluid density).

As soon as the gas flow regime were characterized it was possible to use the Hydraulic analogy in order to identify a complicated fluid problem with an electrical circuit, observing the similarities on the equations and the elements describing the two systems.
In an hydraulic problem the flowing quantity is the fluid that flows through a pipe as the charge current through a wire. Pressure difference on two sides of the pipe is the driving force pushing the fluid through the system as the voltage drop through the friction element (i.e the resistor) allowing the current flow. The storage measure quantity for a fluid is the volume and it is like a capacitor storing the charges, and the friction quantity as the roughness of the pipe permitting the flow as the resistor element in a circuit.
low the pipe is zero.)
The resistance and conductance of a wire, resistor, or other element is mostly determined by two properties:

- geometry (shape)
- material

Geometry is important because it is more difficult to push water through a long, narrow pipe than a wide, short pipe. In the same way, a long, thin copper wire has higher resistance (lower conductance) than a short, thick copper wire.
Materials are important as well. A pipe filled with dirt restricts the flow of water more than a clean pipe of the same shape and size. Similarly, electrons can flow freely and easily through a copper wire, but cannot flow as easily through a steel wire of the same shape and size, and they essentially cannot flow at all through an insulator like rubber, regardless of its shape. The difference between materials is related to their microscopic structure and electron configuration, and is quantified by a property called resistivity.
In addition to geometry and material, there are various other factors that influence resistance and conductance, such as temperature.
Generally speaking, vacuum chambers (like the Vessel in our case) are connected to a vacuum pump via piping. Flow resistance occurs as a result of external friction between gas molecules and the wall surface and internal friction between the gas molecules themselves (viscosity). This flow resistance manifests itself in the form of pressure differences and volume flow rate, or pumping speed, losses. In vacuum technology, it is customary

to use the reciprocal of the flow resistance $1/R$, called conductance. The conductivity has the dimension of a volume flow rate and is normally expressed in $[m^3 s^{-1}]$.
Gas flowing through piping produces a pressure differential Δp at the ends of the piping and is similar to the voltage. The following equation applies:

$$C = \frac{Q}{\Delta p} \tag{2.1}$$

with Q the flow rate. This principle is formally analogous to Ohm's law of electrotechnology:

$$R = \frac{V}{I} \tag{2.2}$$

where Q represents the flow I, C the reciprocals of resistance $1/R$ and Δp the voltage V.
A laminar flow in a gas pipe gives the following formula for the conductance:

$$C^{lam} = \frac{\pi d^4}{128} \frac{1}{L} \frac{1}{\mu} \frac{p_u + p_d}{2} \tag{2.3}$$

with μ the viscosity of the fluid measured in $\frac{dy\ s}{cm^2}$ and the pressures in *bar*. Making the inverse the following formula for the resistance, is given:

$$R^{lam} = \Big(\frac{128\mu}{\pi d^4}\Big) \frac{L}{\frac{p_u + p_d}{2}} \approx \Big(\frac{128\mu}{\pi d^4}\Big) \frac{L}{p_u} \tag{2.4}$$

where in the last equation is the average pressure between the upstream and the downstream one is taken as the upstream pressure because the length in consideration are pretty small, considerable infinitesimal. A Molecular flow in a pipe gives the following formula for the conductance:

$$C^{mol} = \frac{8}{3\sqrt{\pi}} \Big(\frac{2k_B T}{m}\Big)^{\frac{1}{2}} \Big(\frac{A^2}{BL}\Big) \tag{2.5}$$

where B is the priphery of the cross section, L the lenght of the tube, m the mass of the fluid, T the absolute temperature $[K]$ and $k_B \approx 1.38 \cdot 10^{-23}\ JK^{-1}$ the Boltzmann's constant. Using $A = \pi D^{2/4}$ and $B = \pi D$, with D the diameter of the pipe, for the uniform circular cross section and using the molecular mass M instead of m we obtain:

$$C = 3.81 \Big(\frac{T}{M}\Big)^{\frac{1}{2}} \Big(\frac{D^3}{L}\Big) \tag{2.6}$$

where $[D] = m$, $[L] = m$ and $[C] = m^3/s$.
Because of the previous statements the formula for a resistor in a molecular flow regime for a straight pipe, $R^{mol}_{fluidic}$ is given as follows:

$$R^{mol}_{fluidic} = \frac{1}{C} = \frac{1}{3.81} \Big(\frac{M}{T}\Big)^{\frac{1}{2}} \Big(\frac{L}{D^3}\Big) \tag{2.7}$$

The length of the pipe of a pipe with a knee need to be modified because of the increased friction caused by the modification of the shape and so also the formulas of the resistances in both, laminar and molecular, regimes:

$$L \to L_K = K\ D \tag{2.8a}$$

$$R \to R_K \tag{2.8b}$$

where K is a given form coefficient depending on the form of the deformation (some values are shown in table 2.1):

The equivalence between the capacitor and the volume permit the following identification for the capacitance:

$$C_{fluidic} = V_{pipe} \tag{2.9}$$

For chocking in change of cross section flow, what is important is the form of the flow Q, which is given by

$$Q^{chocked} = p_u\ C_D\ A \sqrt{\gamma \Big(\frac{2}{\gamma+1}\Big)^{\frac{\gamma+1}{\gamma-1}}} \sqrt{\frac{M}{RT}} \frac{k_B T}{m} \tag{2.10}$$

Description	Value
∠90° molded	30
∠45° molded	16
∠30° molded	12
∠90° fabricated	24
Equal outlet tee, run/branch	60
Equal outlet tee, run/run	20

Table 2.1: K value for deformations present in SPIDER pipelines

Description	Electrical	Fluid
”through” variable	I (current)	Q (flow)
”across” variable	V (voltage)	P (pressure)
Dissipative element	V = I R	P = Q R
Storage element	I = C $\frac{dV}{dt}$	Q = C $\frac{dP}{dt}$

Table 2.2: Analogy Set

where A is the cross sectional area of flow constriction, C_d a discharge coefficient that can be taken equal to 40,and $\gamma = \frac{C_P}{C_V}$ the heat capacity ratio of the gas. Summarizing, what is found is the possibility to relate relevant fluid dynamic relations and quantities with electrical ones (all in the respect of the measure units which must be in the SI), all the analogies described are summed in table 2.2

An electrical LTSPICE model was built based on the aforementioned hydraulical analogy, and including all the characteristic expressed previously, the different flow regimes. Moreover, during the preliminary operation it was possible to find the relationship between the gas flow through the micrometric valves and the different apertures and so, by comparing the experimental data with the model, it was possible to understand the trend of the valves aperture: the valve completely open, so non-chocked flow, corresponding to the normal flow through the pipes and valve chocked corresponding to different cross sectional area of the flow constriction. The calibration, done for all the shots, has been analyzing the maximum pressure in the Ion-Source and in Vessel carried out of the experimental data and running the model with different cross sectional area, until the right value has been found.
Figure 2.3 presents the electric model of the SPIDER gas piping.

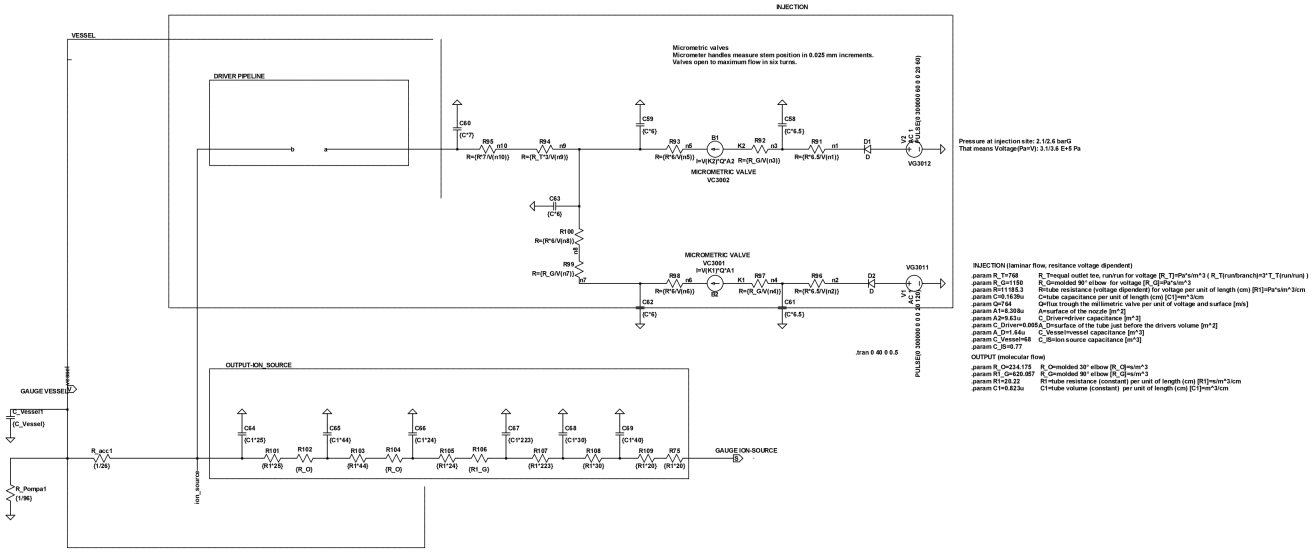

Figure 2.3: LTSPICE Hydraulic Analogy Model

Figure 2.3 shows two generators corresponding to the mechanic valves, than the injection line begins and characterized by laminar flow, the micrometric valves are described by a chocked flow and which the flow

depends on various parameter, but the only free one is the cross sectional area of the flow constriction. After around $4m$ of pipeline, the pipe goes into the drivers (drivers pipeline can be found in appendix) whose represent a big volume in respect of the size of the pipe and so that is possible to identify this point as an other chocked flow with a cross sectional area of the flow constriction as the one of the pipe. At this point the gas is in a regime of molecular flow and it is dissipated in a line corresponding to cryopums and vessel, where it is possible to find the vessel's gauge and in another line that can be called measure line or ion source line at the end of which it is possible to find a gauge, the ion source's one.

2.4 Data Analysis

The shots analyzed and presented in this section findings had a big importance not only at the time, in the first operation of the system characterization, but also they have one in the followings operation because that permit to understand the behavior of the system also with unknown setups just by using the LTSPICE model and the relationships present between the parts of the system.
Figure 2.4 shows one setup of the mechanical and micrometric valves and the superposition of the pressure experimental data with the LTSPICE simulation of the system at the points of the two pressure gauges and the residuals between the two waveforms in output.

2.4.1 Pressure

In order to find the relationship between pressure in vessel, in the ion-source and the inlet one, at the mechanical valves, some shots with different pressures and valves opening were made. That permitted also to find out that one of the micrometric valves, the VC3002, has an additional restriction and so that the outlet flow, in the same condition, is lower than the one coming out from the VC3001.
Studying the behavior of the system to gas injection permitted also the calibration of the LTSPICE model, meaning: it was possible to find the amount of gas flowing from the valves with different turns.
Figure 2.4 shows a setup's example of the mechanical and micrometric valves and the superposition of the pressure taken from experimental data and the one of the LTSPICE simulation. That, of the system at the points of the two pressure gauges. Lastly, the residuals between the two waveforms.

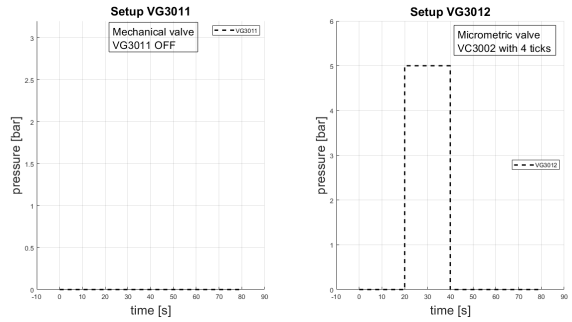

Mechanical valves setup

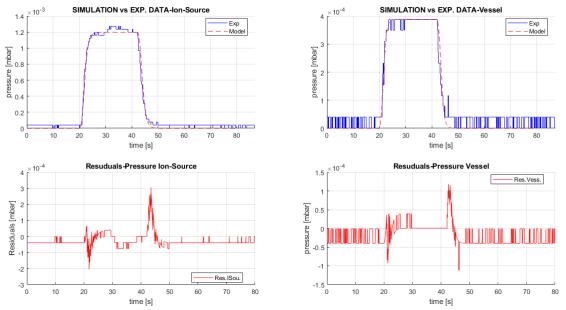

Experiment and simulation comparison

Figure 2.4: Example of Simulation and Experimental data comparison

Errors
Each one of the measures is affected by errors due to the micrometric valve setup and the absolute pressure gauges.

- Micrometric valve: The setup of the ticks and so of the cross sectional area of the flow constriction is a manual operation affected by human error that can be computed as:

$$\Delta_{micro}^{ticks} = \frac{1 \text{ mm}}{\sqrt{12}} \tag{2.11}$$

where 1 mm is the distance between two ticks on the graduated scale of the valve.

- Absolute Pressure Gauge: The gauge is affected by an intrinsic error given by

$$\Delta_{gauge} = 0.08\% \cdot \text{Rdg.} + 125\% \cdot \text{FS} \tag{2.12}$$

where Rdg. means the read value and FS, i.e. sensibility, is equal to 10^{-6} mbar.
In addition to that, the instrument takes points with a frequency of 10 kHz but only if there are variations bigger than its resolution.

The calibration of the LTSPICE model done by comparison between the experimental data and the model results, permits the computation of the cross sectional area of the flow constriction in relation with the ticks of the micrometric valves and with the pressure measured by the gauge in the ion-source.

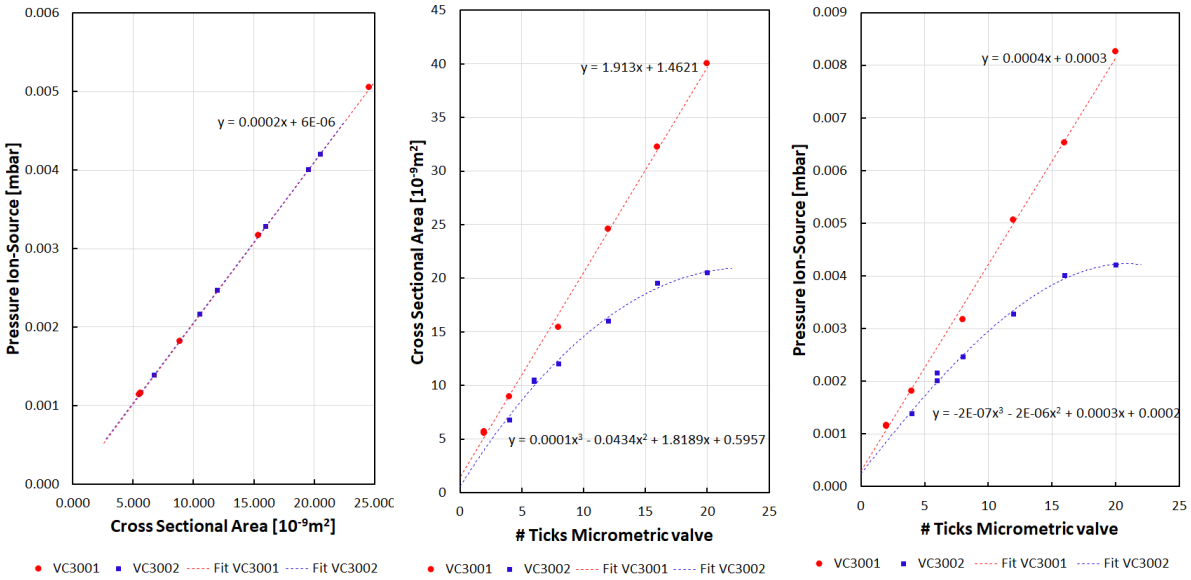

Figure 2.5: LTSPICE Calibration

From figure 2.5 is possible to see the difference between the two valves, in particular it can be seen that the microvalve VC3001 present a linear behavior of the ticks on the valve with respect of the pressure in the ion-source. The other valve, VC3002, present an other chocking that keep the system away from maintaining the linear relation between pressure and the valve ticks. Beginning from 12 ticks on, the linear relation become a polynomial relation with a saturation point, i.e. increasing the aperture of the microvalve will not affect the gas flux and so the pressure reached in the ion-source.
The calibrated model seems to reproduce in good agreement the experimental data. In figure 2.6 a plot of an experimental operation and the relative operation of the model.

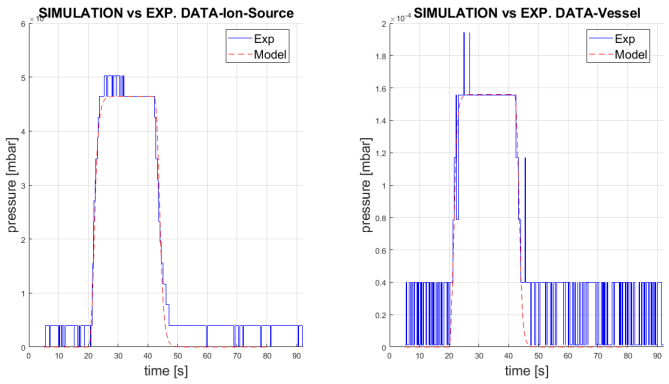

Figure 2.6: LTSPICE and experimental shot

The agreement between the LTSPICE simulation and the experimental data can be computed with the analysis of the normalized residuals. The analysis shows that the average of the residuals in every shot lies around 0 mbar/mbar. This happens with both the pressures, in the ion-source and in vessel as shown in figure2.7 and referenced to figure 2.6. That means that the model is well reproducing the real operations both in transitory and stationary phase

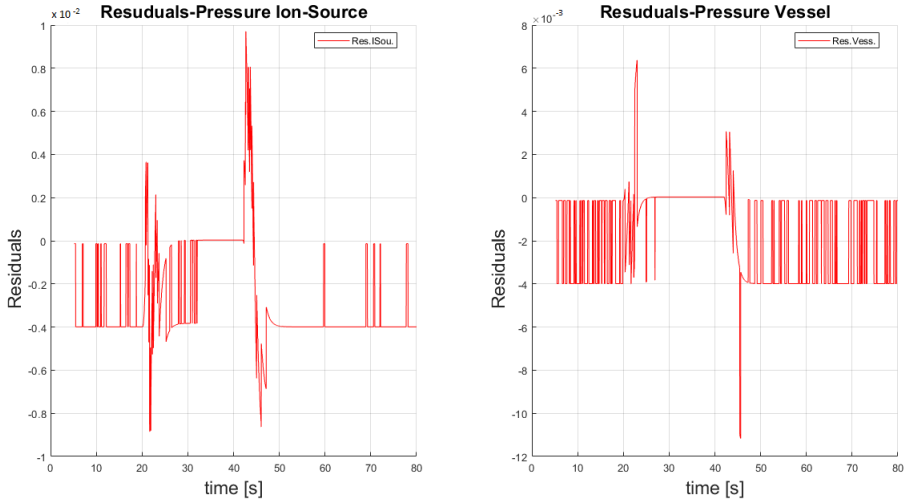

Figure 2.7: RESIDUALS

Both Experimental Data and Model shows that the relation between ion-source's and the vessel's pressure is linear due to the constance of the conductance. It is possible to write the relation $Q = C(p_{ion-source} - p_{vessel})$ or $p_{ion-source} = \frac{Q(\#)}{C} + p_{vessel}$ where the gas flux depend on the ticks of the micrometric valve.

Figure 2.8: Relation pressure in vessel and in ion-source

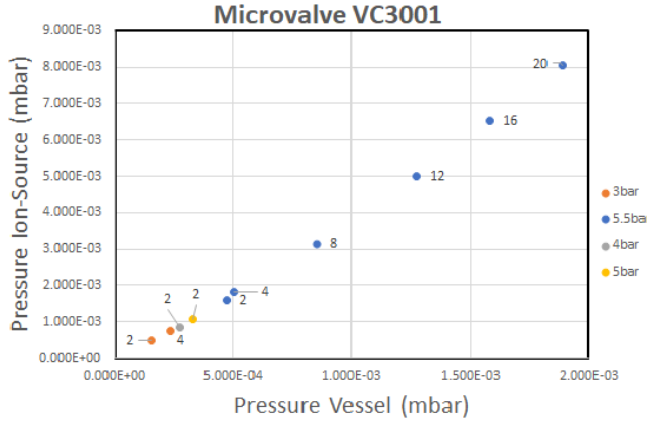

Figure 2.9: (a) At fixed inlet pressure and different # ticks of micrometric valve

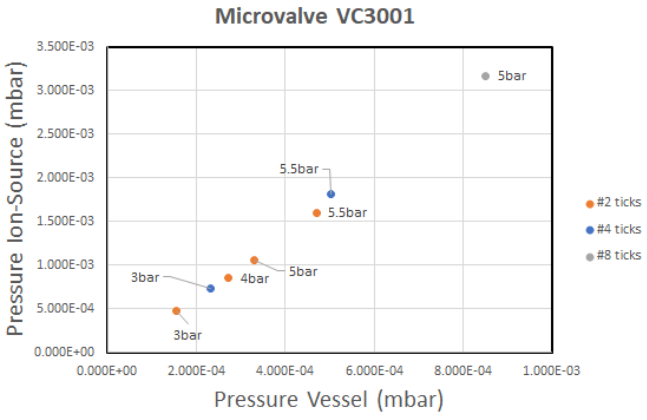

Figure 2.10: (b) At fixed # ticks of micrometric valve and different inlet pressure

Studying the pressures in input and the one in the ion source is possible to find a linear relation between the two, at fixed # turns of the micrometric valve

and also a relation between the two variables and the ticks of the micrometric valve considered as a dipendent parameter.
Since we consider the gas flux a variable dependent on the ticks of the micrometric valve, from the equation $Q(\#) = C(p_{Inlet} - p_{ion-source})$ is possible to obtain a relation $\frac{p_{Inlet}}{p_{ion-source}} = \frac{1}{\frac{Q*\#}{C}-1}$ The resulting fitting curves have an equation like: $y = \frac{a}{b \cdot x - 1}$

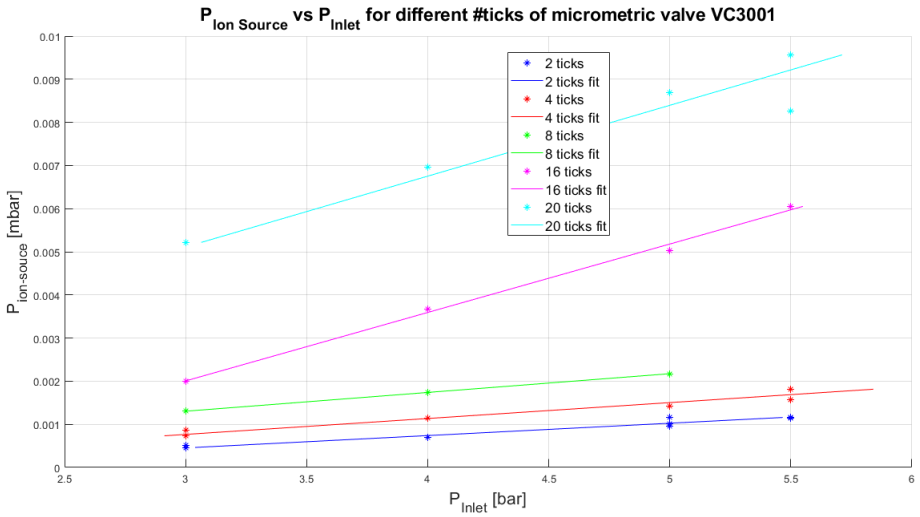

Figure 2.11: P_{Inlet} vs $P_{ion-souce}$

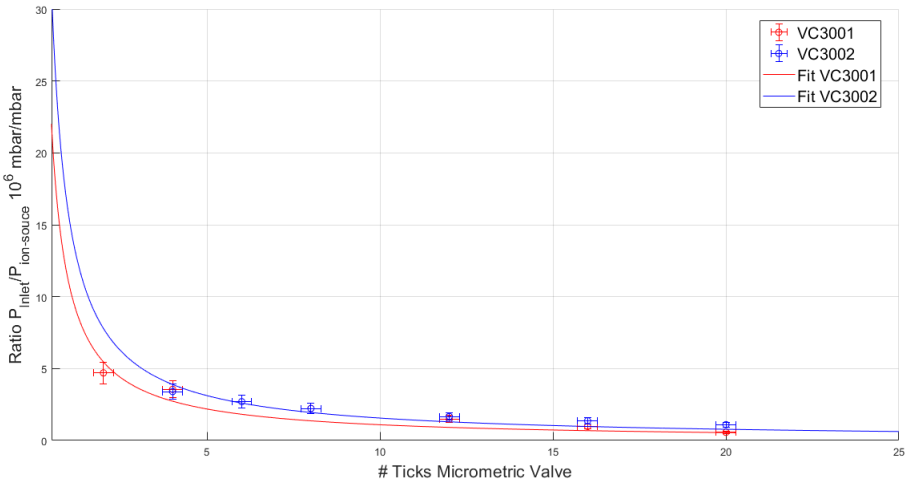

Figure 2.12: Ratio $\frac{P_{Inlet}}{P_{ion-souce}}$ vs # Micrometric Valve Ticks

Valve	Coefficient	Value	σ
VC3001	a	2.055	0.9593
	b	1.881	0.0878
VC3002	a	1.023	0.2299
	b	0.657	0.1476

2.4.2 Characteristic Time

The LTSPICE model and the experimental data show that the time the gas need to reach the maximum pressure is larger for the ion-source than for the vessel, because of the longer path the gas needs to go across before reaching the pressure gauge.

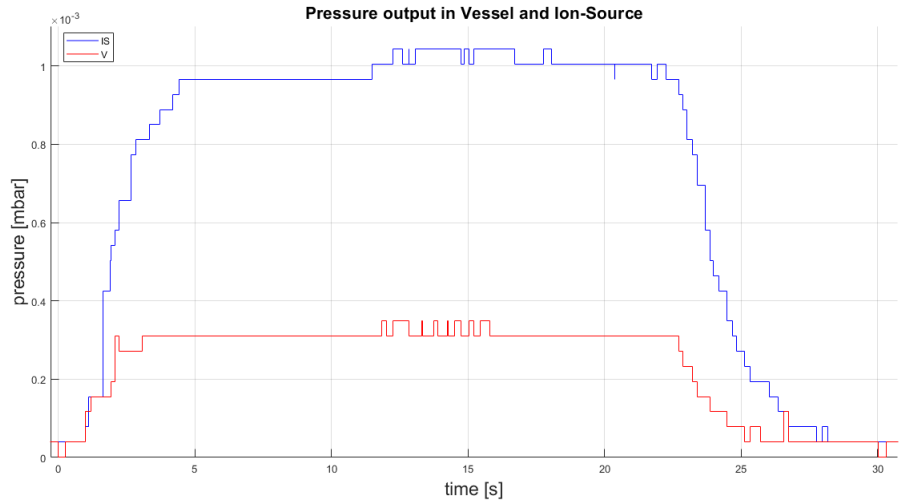

Figure 2.13: Visualization with a shot of the time difference between vessel and ion-source

Defining the characteristic time as the time at which the pressure reaches $1 - 1/e$ of its maximum value, it is possible to see both experimentally and from the simulation that this time remains the same by changing the input pressure or changing the valve ticks. Also the characteristic time difference between ion-source and vessel remains constant (the ion-source characteristic time is smaller).

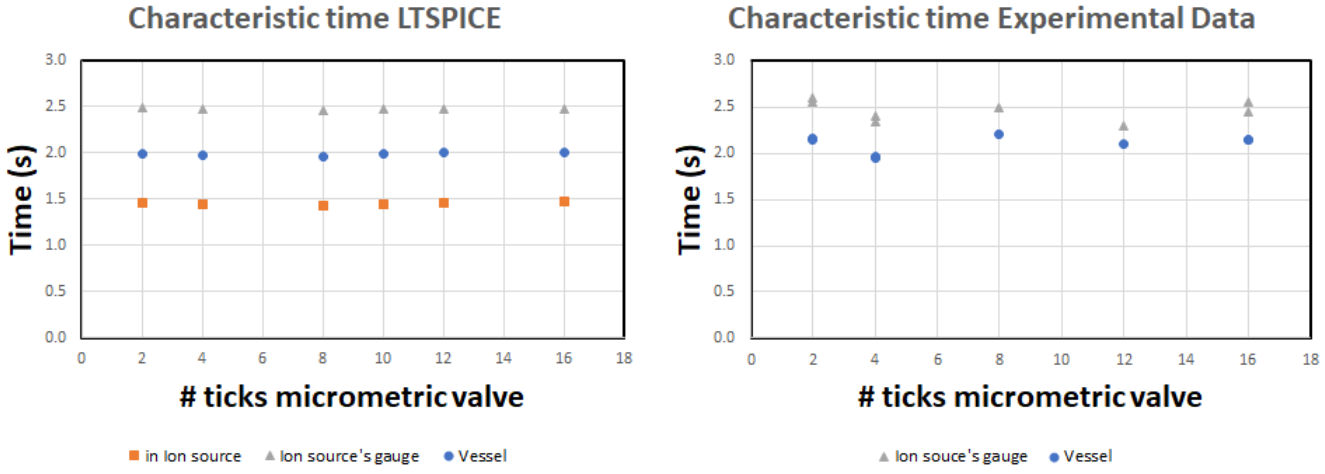

Figure 2.14: Characteristic Time vessel and ion-source

Experimental data and the model present the same characteristic time within the human error, in particular $\tau_{ion-source} = 2.47$s and $\tau_{vessel} = 2.15$s and so $\Delta\tau \sim 320$ms

2.4.3 Gas Flow

The importance of the conductance lies in the fact that it is a constant parameter with or without plasma. The pressure cannot be taken as a reliable parameter because it is a parameter dependent on the temperature and so

it increases when a plasma is present.
The amount of gas flowing and the conductance into the piping system can be estimated in three different ways:

- Injection valve Test: preliminary test of the valves before the complete building of the entire piping system.
- Cryopumps: assuming the nominal pumping speed, $S = 96/8$ m^3/s for each one of the 7 operating pumps.
- Linear extrapolation of the micrometric valves' behavior.

The three ways give the following results:

Inlet pressure: 2 bar	Gas Flux [Pa · m^3 / s]	Conductance [m^3 / s]
Injection valve test	0.95	30.74
Cryopumps	1.30	42.14
Linear	1.30	32.97
Inlet pressure: 4.5 bar	Gas Flux [Pa · m^3 / s]	Conductance [m^3 / s]
Injection valve test	1.70	30.74
Cryopumps	1.96	42.36
Linear	1.96	33.07
Inlet pressure: 6 bar	Gas Flux [Pa · m^3 / s]	Conductance [m^3 / s]
Injection valve test	2.70	39.13
Cryopumps	2.60	37.74
Linear	2.60	29.53

Those value must be compared to the constant conductance $C = 26.80$ m^3/s evaluated with an AVOCADO simulation of the complete SPIDER beam source.

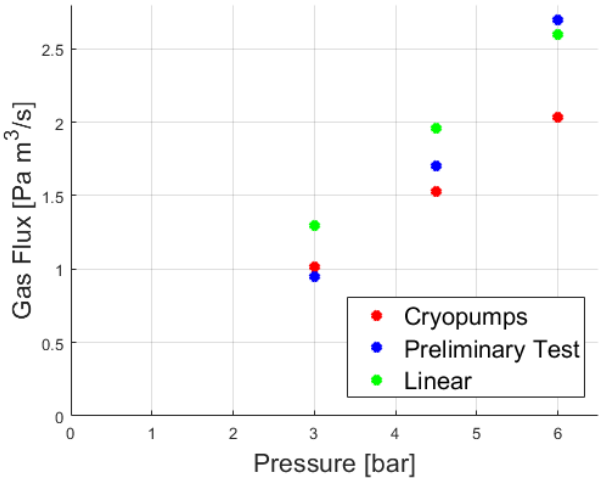

Figure 2.15: (a) Inlet Pressure and Gas Flux

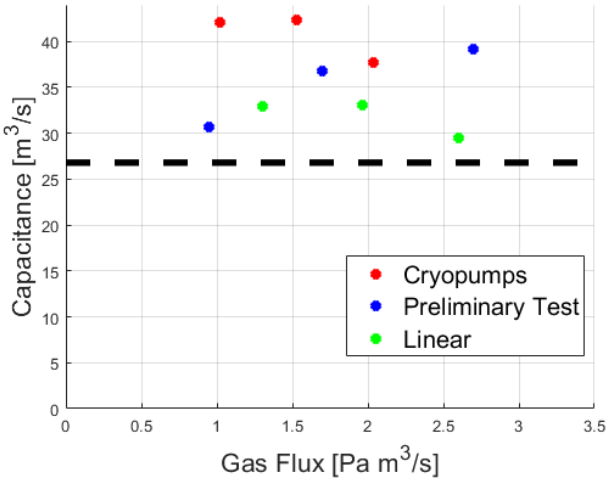

Figure 2.16: (b) Gas Flux and Conductance

The gas Flux follows a linear behavior with respect to the inlet pressure, as expected, and the three different calculation seem to be in good agreement with each other. The vessel conductance calculated with the three methods returns different values depending on the method used to its calculation and it also differs from the constant value calculated with the AVOCADO simulation (the black line at 26.8 m^{3}s^{-1}).

Chapter 3

Filaments

As inductive coupling of the RF power alone is unable to initiate the plasma reliably because the Faraday shield prevents the capacitive coupling, a small starter filament is necessary to ignite the plasma. Therefore eight starter filaments (one per driver) were installed in SPIDER in order to help the RF Source in the starting up of the plasma. The starter filaments are connected in parallel at the source and fed by a single pair of conductors. The filaments control is an ON/OFF type connected to all the eight filaments.
A Filament Bias Power Supply (ISFB) is used, in order to bias the starter filaments with respect to the body of the source.

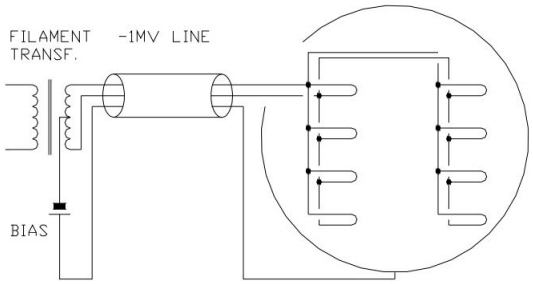

Figure 3.1: Circuit layout of starter filaments and bias

3.1 Tungsten Filaments

One of the main sources of free electron is a hot filament. Electrons are emitted from hot cathodes (usually tungsten filaments) and then accelerated into the source body, where they create a plasma by ionization of the background gas. Because of sputtering and evaporation, the tungsten filament lifetime is finite, so these sources require regular maintenance. Tungsten is a metal having the highest melting temperature ($T_F = 3695\ K$) and the filament is essentially a resistance heated by Joule effect. In SPIDER the filaments are single coiled and they are made also with a 3% of Rhenium, so that it will have superior electrical resistivity and mechanical strength and also non-sag property when operating at high temperature, or under vibration. The closer the spacing of the coils, known as the pitch, then the hotter the filament can operate.

A metal consists of a lattice of atoms arranged in a regular pattern called crystalline structure, each with an outer shell of electrons that freely dissociate from their parent atoms and travel through the lattice, the delocalization of valence electron allows the solid to conduct an electric current. When a voltage, an electrical potential difference is applied across the metal, the resulting electric field causes electrons to drift towards the positive, terminal. So that electrons, acquire kinetic energy. When the electrons collide with ions in the conductor lattice, the particles are scattered; their direction of motion becomes random rather than aligned with the electric field, which constitutes thermal motion. Thus, energy from the electrical field is converted into thermal energy. Most

metals have resistance. The amount of resistance is thus caused by mainly two factors. Firstly it is caused by the temperature and thus speed of vibration of the crystal lattice. The temperature causes irregularities in the lattice. Secondly the impurity of the metal is relevant as different ions cause irregularities too. The larger the cross-sectional area (Σ) of the conductor, the more electrons per unit length are available to carry the current. As a result, the resistance is lower in larger cross-section conductors. The number of scattering events encountered by an electron passing through a material is proportional to the length (L) of the conductor. The longer the conductor, therefore, the higher the resistance. Different materials also affect the resistance. So that is possible to associate a resistance to the metal with a form

$$R = \rho \frac{L}{\Sigma} \tag{3.1}$$

The factor ρ is called resistivity, it quantifies how strong a given material opposes the flow of electric current. Metals are characterized by a low resistivity that however changes with the temperature and in general the for a metal, it increases linearly with the temperature as $\rho = \rho_0(1+\alpha T)$ with α, an empirical parameter characteristic of each metal.
The transformation of kinetic energy into thermal energy is called Joule heating and states that the power of heating generated is given by

$$P_J = R\, I^2 \tag{3.2}$$

At each temperature variation always correspond an exchange of heat between bodies (one can be a metal and the other a body close to it, but it is not necessary). The heat exchange in the absence of a medium, is called radiation. The radiation power follows the Stefan-Boltzmann's law stating that the total radiant heat energy emitted from a surface is proportional to the fourth power of its absolute temperature. Thus we can write for the radiation power

$$P_R = \varepsilon S \sigma_B\, T^4 \tag{3.3}$$

where ε is the emissivity of the specific material describing the fraction of radiated energy of the material with respect of the one radiated by a black body ($\varepsilon = 1$), S the exposed surface, σ_B is the Stefan-Boltzmann's constant

$$\sigma_B = \frac{\pi^2 k^4}{60\hbar^3 c^2} = 5.67\ 10^{-8} W m^{-2} K^{-4} \tag{3.4}$$

Considering those two types of thermal power involved, as usually happens in an experiment involving heated conductors, it is possible to write a differential equation for the steady flow of heat across an element, dx in thickness and at a temperature T, of a filament:

$$-\frac{d}{dx}\left(\Sigma k_T \frac{dT}{dx}\right) = \frac{c^2 \rho_T}{\Sigma} - 2\pi r_{filament}\, \sigma_B \varepsilon (T^4 - T_0^4) \tag{3.5}$$

with the assumption that for the filament in use in SPIDER the usual equation

$$R = \rho_0(1 + \alpha \Delta T)\frac{L}{\Sigma} \tag{3.6}$$

for the resistance is not accurate but holds the following relation:

$$\frac{R_2}{R_1} = \frac{\rho_2}{\rho_1} = \left[\frac{T_2}{T_1}\right]^{\beta} \tag{3.7}$$

and the parameter β for a wire in tungsten with 3% of rhenium is equal to 0.94.

When a conducting body, as a metal, is heated at a sufficiently high temperature, electrons are emitted from its surface. This phenomenon is known as thermionic emission. The electrons available for emission are generally assumed to be the same as those available for conduction, the free/valence electrons. The minimum amount of energy needed to the process is called work function and it is characteristic of the material, in a microscopical view it is defined as the potential rise of an electron as it moves from the Fermi level to a potential V=0. The

experimental law of Richarson and Dushman describe the relation between the emission current density j and the cathode temperature T

$$j_S = A_g\, T^2\, e^{-W/k_B T} \tag{3.8}$$

where $A_g = \lambda_R\, A_0$ is the Richardson constant, in which λ_R is dependent on the cathode material, and given by

$$A_0 = \frac{4\pi mek^2}{h^3} = 1.20173\ 10^6 A\ m^{-2}\ K^{-2} \tag{3.9}$$

The Boltzmann constant k_B is a measure of the relative probability for an event requiring energy W (work function) in a system at temperature T.

For a high-voltage sheath, the current to the electrode is almost all ion current. Provided the ion motion in the sheath is collisionless, then the steady self-consistent ion density is not uniform, but rather is described by the Child–Langmuir law of space-charge-limited current in a planar diode. As the emitted particles come out from the cathode they create a cloud of negative charge and so an electric field opposing to the one on the material. in a very high vacuum the space charge of the electrons limits the current that can flow from a hot cathode to a positively charged anode so that beyond a certain point an increase in the temperature of the cathode causes no further increase in current. When the cathode and anode are long coaxial cylinders and a plane polarized with respect of it, the current limited by space charge is given by

$$j_{C-L} = \frac{8\pi\varepsilon_0}{9}\sqrt{\frac{2e}{m}}\frac{V^{3/2}}{(r\beta^2)} \tag{3.10}$$

Here j is the electron current per unit length along the axis, V the, anode, voltage at any point P, r the radius at P, e and m the charge and mass respectively of an electron. β is a quantity of zero dimensions, r_c the radius of cathode: the factor β can be found in tables and has different value depending on the value of the ratio r/r_c.

3.2 Experimental Characterization of filaments

For the experimental characterization of the filaments, only seven filaments were available, and it was used an electrical circuit like the one shown in figure 3.2. What has to be noticed is that during the characterization the filaments where yet in place inside SPIDER's drivers.

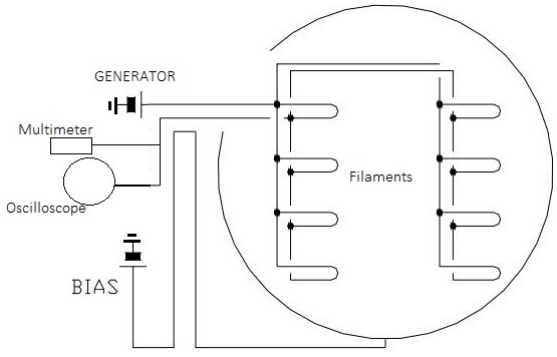

Figure 3.2: Circuit scheme for the filaments characterization

The use of a controlled generator and oscilloscope permitted to identify the relation between the circulating current and the voltage difference at the ends of the circuit. It was possible to find the resistance of the hot filament, using the Ohm's Law $\Delta V = R\, I$, and using the equation 3.7 the temperature reached in the operation. During the operations it has been necessary to add a resistor in set with the filaments in order to limit the emitted current by thermoionic emission and to bias the starter filaments with respect to the body of the source moreover, in order to decrease the filament temperature for increase its life.

3.3 Data Analysis

The filament in use are coiled tungsten mixed with a 3% of rhenium, a view of the filament is shown in figure 3.3.
In order to undertand the filaments behaviour some experimental curves have been carried out by using different applied voltage to the electrical circuit and different bias voltages.

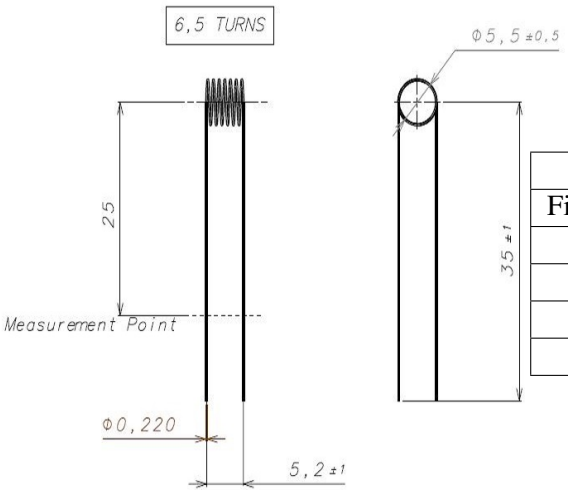

Description	Symbol	Value
Filaments and cable resistance @ 293K	R_0	110 mΩ
Applied Voltage	V	20 Vrms
Resistance-temperature coefficient	β	0.94
Resistivity temperature coefficient	α	3.30910^{-3}
Wire emissivity	ε	0.22

All the data are expressed in mm

Figure 3.3: View and Characteristics of the Filaments

The experimental curve $V_{fil}(I_{fil})$ is the first step to study the filaments behavior: the Ohm's law $\Delta V = R \cdot I$ show that the proportional coefficient between the applied voltage and the current in the system is the resistance. The resistance that appears in the Ohm's law is the sum of the resistance of the cable, that can be considered constant i.e. not subjected to the ohm's heating, and the resistance of the filaments in parallel, that depends on the filament temperature with the relation 3.7.

Figure 3.4: Voltage and Current relationship

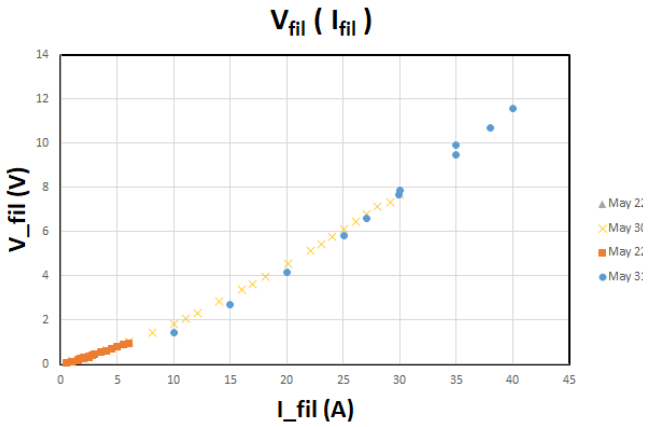

(a) With no additive resistance

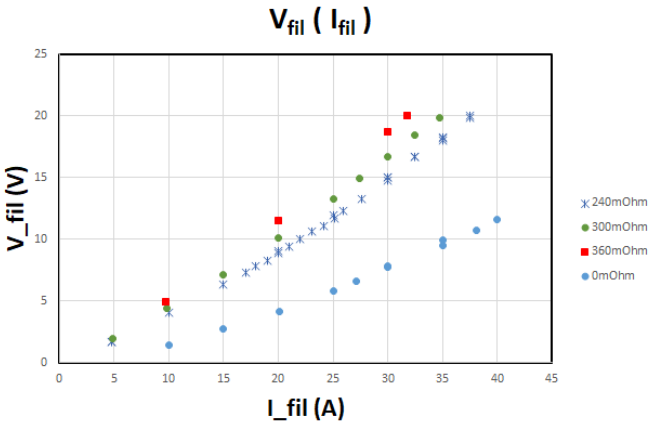

(b) With different additive resistances

As it is possible to see in figure 3.4 the relation between the voltage and the current is not exactly linear due to the not linear relation between the resistance and the heating temperature of it. During the operations have

been used different additional resistors in series with the cable, in particular with values 240 mΩ, 300 mΩ and 360 mΩ. The curve $V_{fil}(I_{fil})$ follows the same non linear trend in all four situation with a slope decreasing with increasing with the value of the additional resistor, and so an increasing limitation on the filament current.

Combining the previus result, using the Ohm's law $\Delta V = R\ I$ in order to carry out the resistance of the filament and using the relation 3.7 between the temperature and the resistance is also possible to see that the curve $T_{fil}(R_{fil})$ almost follow a linear trend and independent from the additional resistor, due to the fact that coefficient β is almost 1 ($\beta_W = 0.94$).

Figure 3.5: Temperature and Resistance relationship

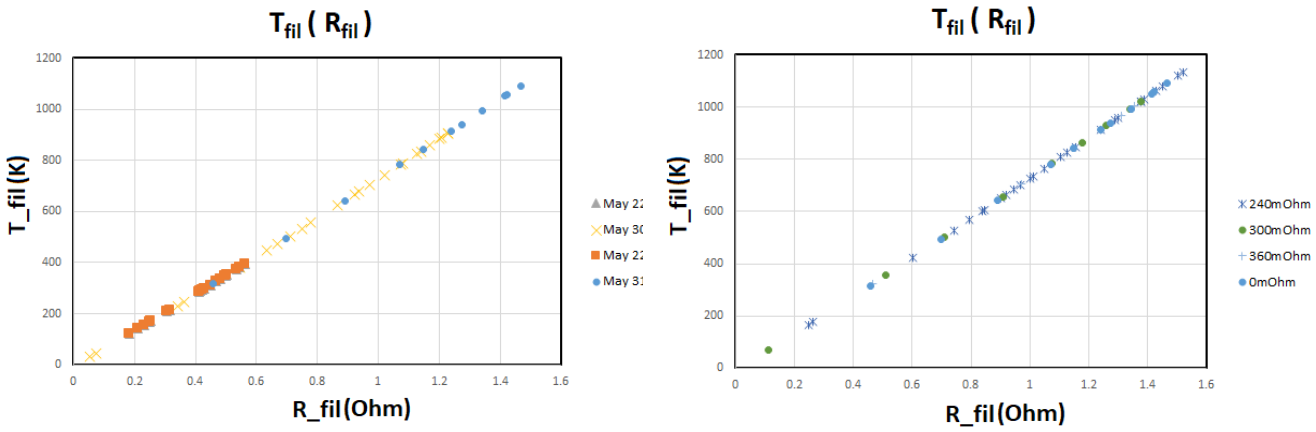

(a) With no additive resistance

(b) With different additive resistances

An other interesting curve is the one relating the filament current and the temperature.

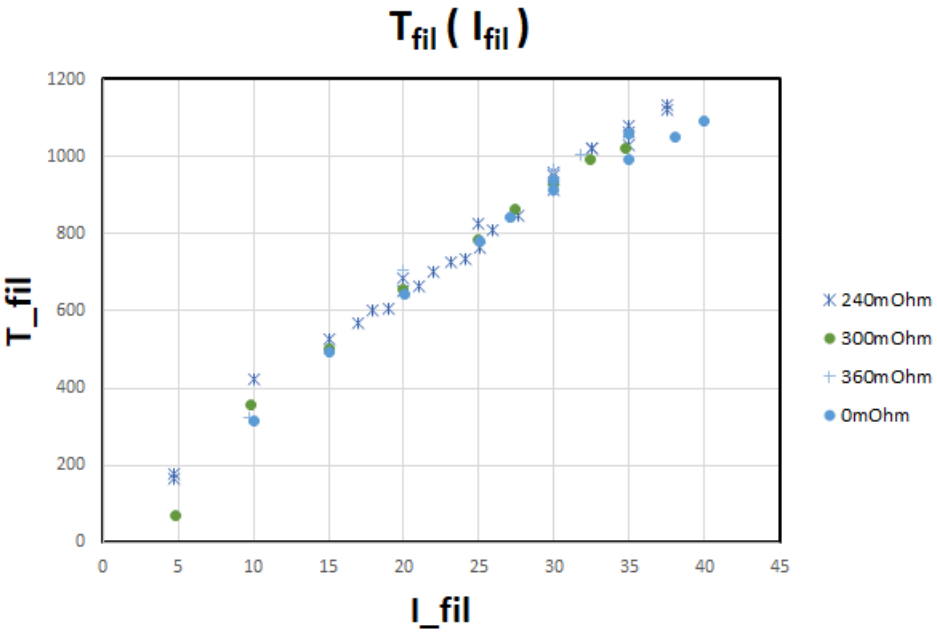

Figure 3.6: Filament Temperature and Current relationship

With a PYTHON program it has been possible to solve the differential equation 3.5 and to find the temperature distribution along the filament for different filament currents. Because of its shape (negletting the different radiating contributes of the coils), the temperature distribution along the filament is not uniform but follows the trend shown in figure 3.7.

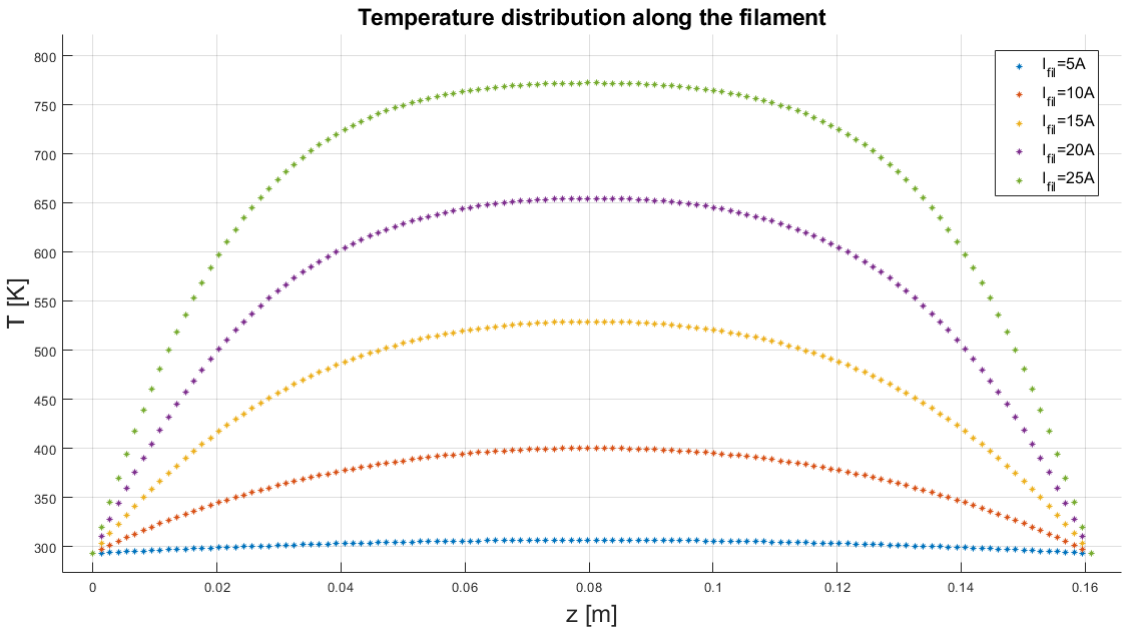

Figure 3.7: Temperature distribution along the filament

The agreement between the experimental data and the python simulation is good but not optimal, in order to solve the differential equation it has been necessary to use the linear dependence between the resistance and the temperature with the formula $R = R_0(1 + \alpha\Delta T)$ and to choose a value for α while for the experimental data the relation between resistance and temperature wasn't linear and dependent on the parameter β. (α and β are experimental values and as such affected by errors whose magnitude depend on the method and the instruments used).

The emitted electron current is represented by the following relation from Child-Langmuir law: $I_{bias}(V_{bias})$

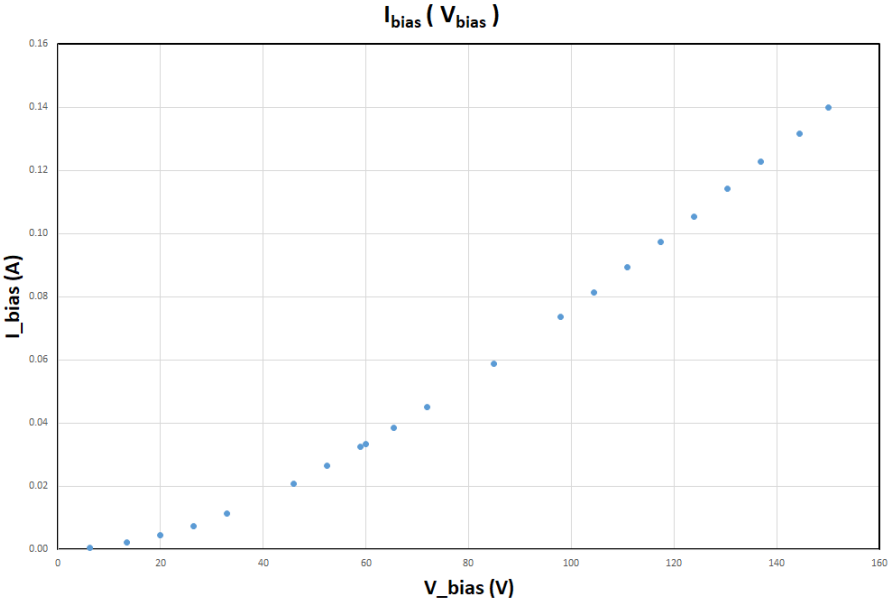

Figure 3.8: Bias Voltage and Bias Current relationship

The data are in very good agreement fitted by the function: $I_{bias} = V_{bias}^{3/2}\ 7.6783\ 10^{-5}$ A/V$^{2/3}$, where the constant factor come from equation 3.10 and using $\beta^2 = 1.55$.
It is useless to heat at 3000K the filament if the maximum extractable current is anyway limited by the spatial charge (Child Langmuir). Because of this fact, it has been decided to place a resistor in serie with the

filaments that limits the current on the filaments in order to do not go at useless high temperature for a given available bias voltage i.e. $I_{ChildLangmuir} = f(V_{bias}, fil)$, $I_{Richardson} \leq I_{ChildLangmuir}$ from which I evaluate $I_{max,fil} = I_{fil}(T_{fil}(I_{Richardson}))$.

From figure 3.9 it is possible to see that for a fixed bias voltage (in figure: $V_B = 100$ V). even with different

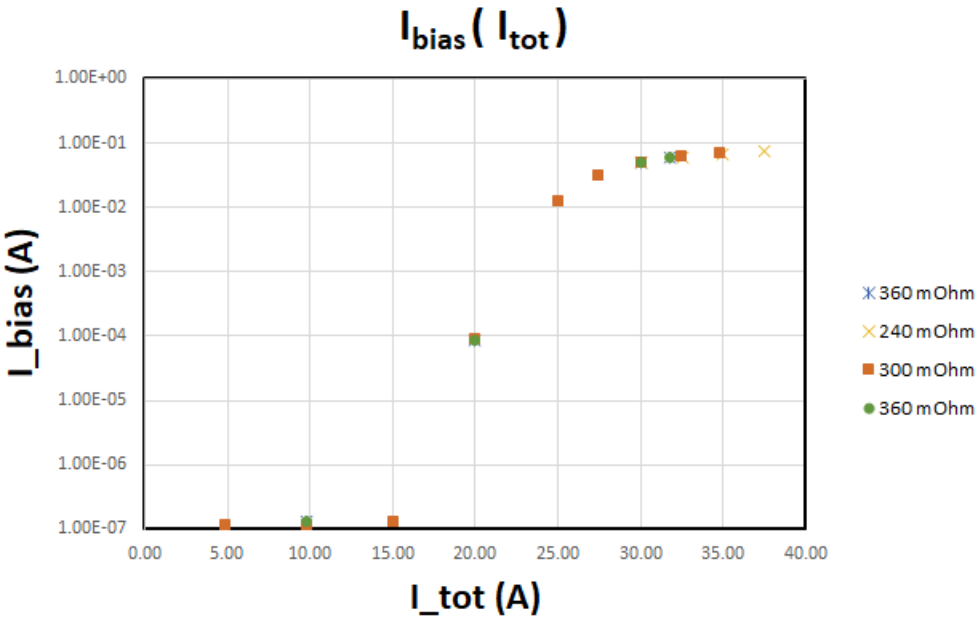

Figure 3.9: Bias Voltage and Total Current relationship

resistors, the emitted electron current show the same behavior with respect of the current in the circuit. In particular result $I_{emitted} = min\{I_{Richardson;}\, I_{ChildLangmuir}\}$, $max(I_{emitted}) = I_{ChildLangmuir} = 0.077$ A.

Chapter 4

Parameters for plasma ignition

The independent study of the three parameters involved in the plasma ignition, permitted to reach the 6^{th} of June an operational condition with a sustainable plasma.
In a RF source, like SPIDER, a coil is wrapped around an insulated section of the source wall (the Driver). If some gas (Hydrogen or Deuterium) is puffed inside the source, as the coils are fed with a very high Radio-Frequency (1 MHz) field, a high frequency current is then driven in the plasma and collisions ensure that the RF power sustains the plasma. The initial plasma has to be formed thanks to the presence of energetic electrons, which are generated by dissociative ionization of the initial gas (H_2) and directly given by the initial seeding coming from the filaments. The electrons, accelerated by the RF fields, become sufficiently energetic to cause ionization and dissociation, whose rate coefficients are strongly dependent on the electron temperature itself. The ionized plasma constituted by the main species e^-, H, H_2, H^+, H^{2+}, H^{3+}.

4.1 Main issues in first operations

The system could sustain only a fixed gas flow before the cryopumps overheat. The cryopumps when stopping a particle, they assorb its energy, the cryo system can sustain until a certain value of heat per unit of time (power) before to go in protection. In this situation the operation becomes uncontrollable and for the followings operations at least a day to reset the system is needed.

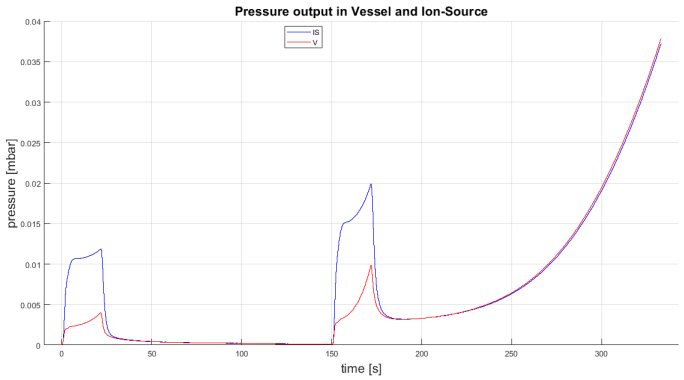

Figure 4.1: Pressure in Vessel and Ion-Source in cryopums oversaturation operation

RF breakdowns in the dome outside of the drivers occurred, i.e. the discharge did not happen in the dome of the vessel between the drivers and the acceleration and extraction grids but it happened in the back side of the RF coils. This event can lead to breakage of the systems components and also of the filaments. In order to decrease the probability of this to happen has been decided to set a reasonable maximum at the RF operational power.

Figure 4.2: Capture of a discharge in the dome outside of the drivers

4.2 Ignition

As soon as the first ignition was reached the main goal became to investigate the best combination of the three controllable parameter, meaning the amount RF power and a suitable wave form for the pulse as the number of generator switched on, the gas flow and pressure, the time of switch ON/OFF of the filaments and the PG current controlling the magnetic filter field. In Figure 4.3 is represented the variation in time of the first three parameters during an operation with a plasma ignition that happened at 0.07s.

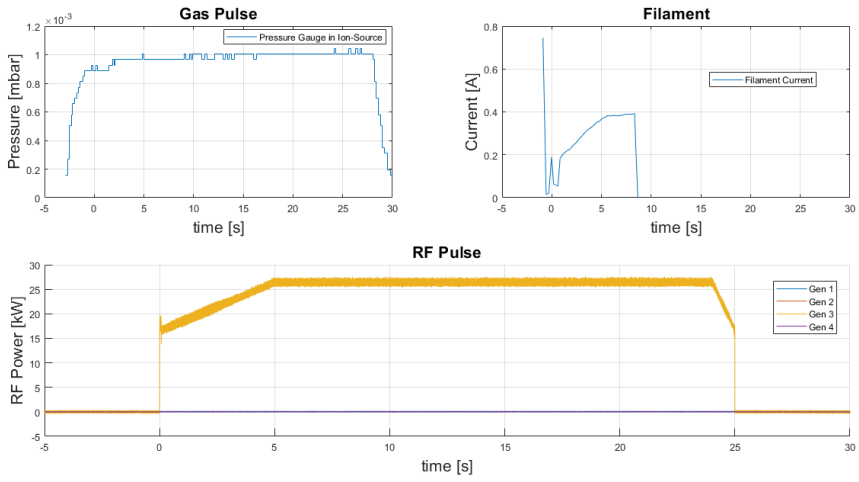

Figure 4.3: Operation with Plasma at 0.07s

It is possible to visualize the plasma ignition by looking at the cameras placed around SPIDER vessel but in a more physical way, by studying the intensity of the eight plasma light photodiodes which are placed one per driver.

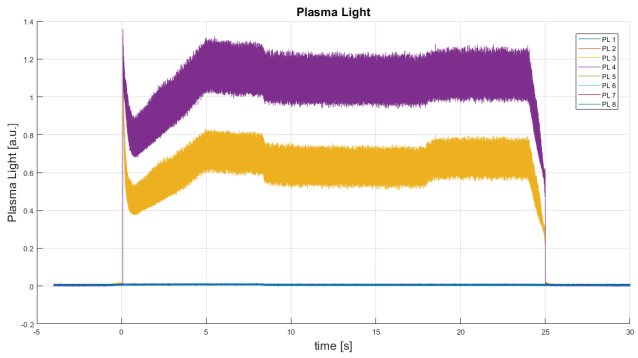

Figure 4.4: Plasma Light data corresponding to the previous shot

4.2.1 Results

This section shows the resulting correlation between the values of the three controlled parameters at the moment of plasma ignition.
In the following operations the filament were setup to switch on at 0 second and to stay ON for 8 seconds and biassed at 60 V in respect of the ground. The gas flow was the result of the gas flowing trough the micrometric valve VC3002 with an opening of 12 ticks.

The operations showed that for increasing ion-source pressure the time of ignition decreases. This can be connected directly to the fact that more pressure means also that the injected gas (which flow is constant due to the microvalve setup) is more and that higher pressure increase the probability of collision and so also of ionization.

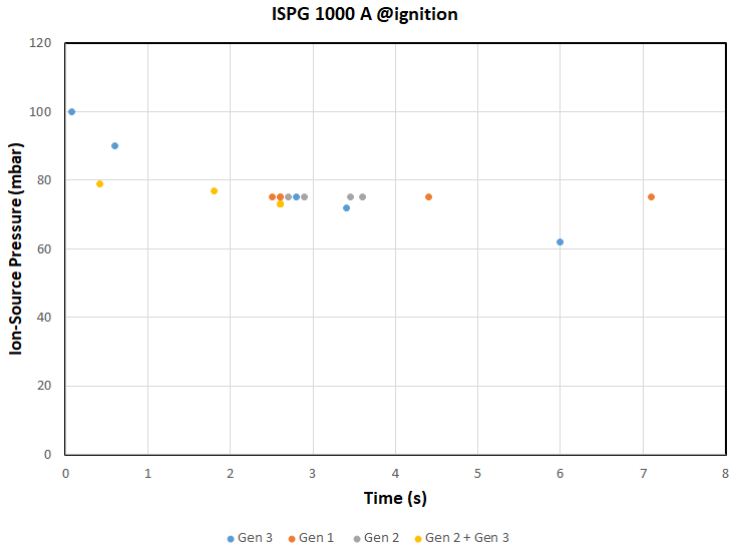

Figure 4.5: Relation Ignition Time and Pressure

The main relations that have to be investigated are the ones relating the various parameters at the ignition time, in order to find the best way to ignite plasma and later to sustain itself the longest.

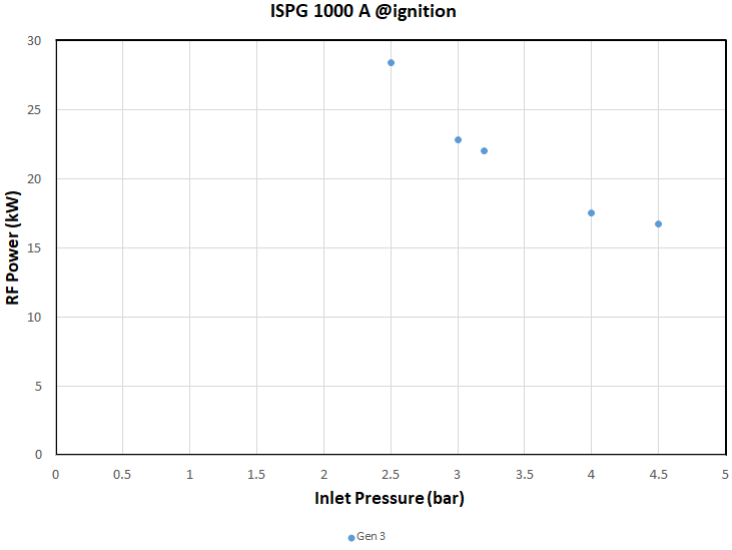

Figure 4.6: Relation Inlet Pressure and RF power at ignition

Figure 4.6 show a behavior like the Pashen Curve i.e. $V_b = V_b(p\,d)$ electrical potential of discharge as a function of the pressure and the distance between the electrodes. The principal difference between the experimental behavior found and the Pashen Curve lies in the fact that the plasma ignition occur in RF with electrons-seed. It is anyway possible to find the configuration of minimum of the function $P_{RF}(P_{in})$. With respect of such configuration lowering the pressure mean that there will be more target but the same amount of electrons and so less products which implies less current but what permit the ignition is the electron multiplication (Thownsend multiplication), so that it can be also possible to do not reach the ignition. On the other hand, if the pressure is strongly increased the mean free path decrease and as a consequence the electrons gather less energy and the probability of ionization strongly decrease.

Generator 3, as can be also seen in the following figure, do not ignite with PG current lower than 300 A, in particular the slope $P_{RF}(I_{PG})$ is almost parallel to the y-axis for PG currents around the value of 300 A. The combination of generator 2 and 3 shows something else: it is possible to ignite, thanks to generator 2 also without the magnetic filter coming from the plasma grid current. The fitting function, in this last case is almost a curve parallel to the x-axis.

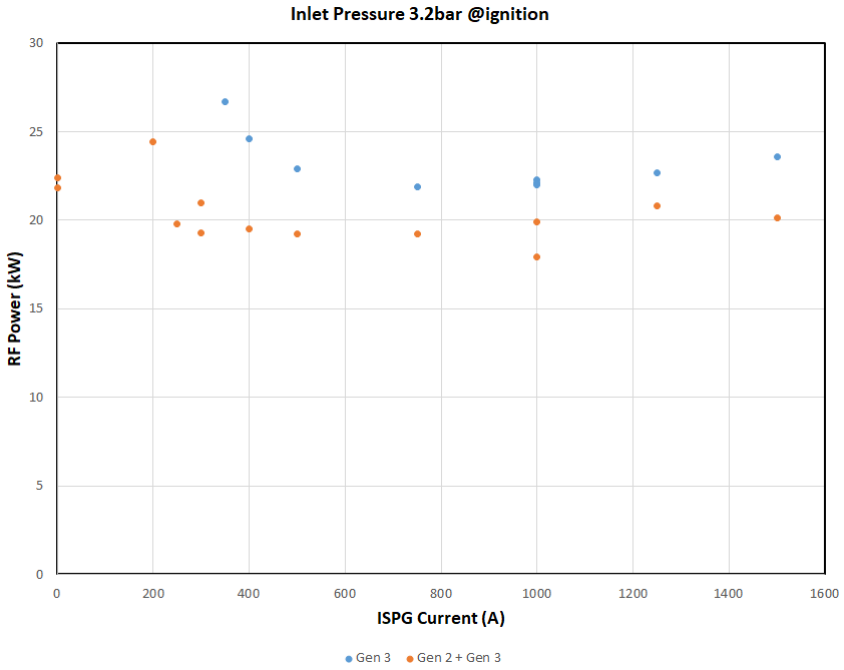

Figure 4.7: Relation PG Current and RF power at ignition

Chapter 5

First Plasma characterization

5.1 Plasma Light

In the SPIDER experiment are installed eight plasma light each positioned in one of the eight drivers. The system of the Plasma Light detector modules is based on Photodiode-Amplifier which combines a photodiode with an operational amplifier.A photodiode is a p–n junction or PIN structure. When a photon of sufficient energy strikes the diode, it creates an electron-hole pair. This mechanism is also known as the inner photoelectric effect. If the absorption occurs in the junction's depletion region, or one diffusion length away from it, these carriers are swept from the junction by the built-in electric field of the depletion region. Thus holes move toward the anode, and electrons toward the cathode, and a photocurrent is produced.
Due to three different mechanisms the plasma emits Bremsstrahlung, recombination and line radiation (including photons). The light signal collected by the photodiode from the experiment gives information about the plasma intensity, its spatial position and also the information about the moment the plasma has been ignited.
The plasma lights' signal of an operation with two of the four RF generator switched on, present the form shown in figure 5.1. It is noticeable that the form of the photodiode signal follows the wave form setted up for the RF generator which the detectors are attached to.

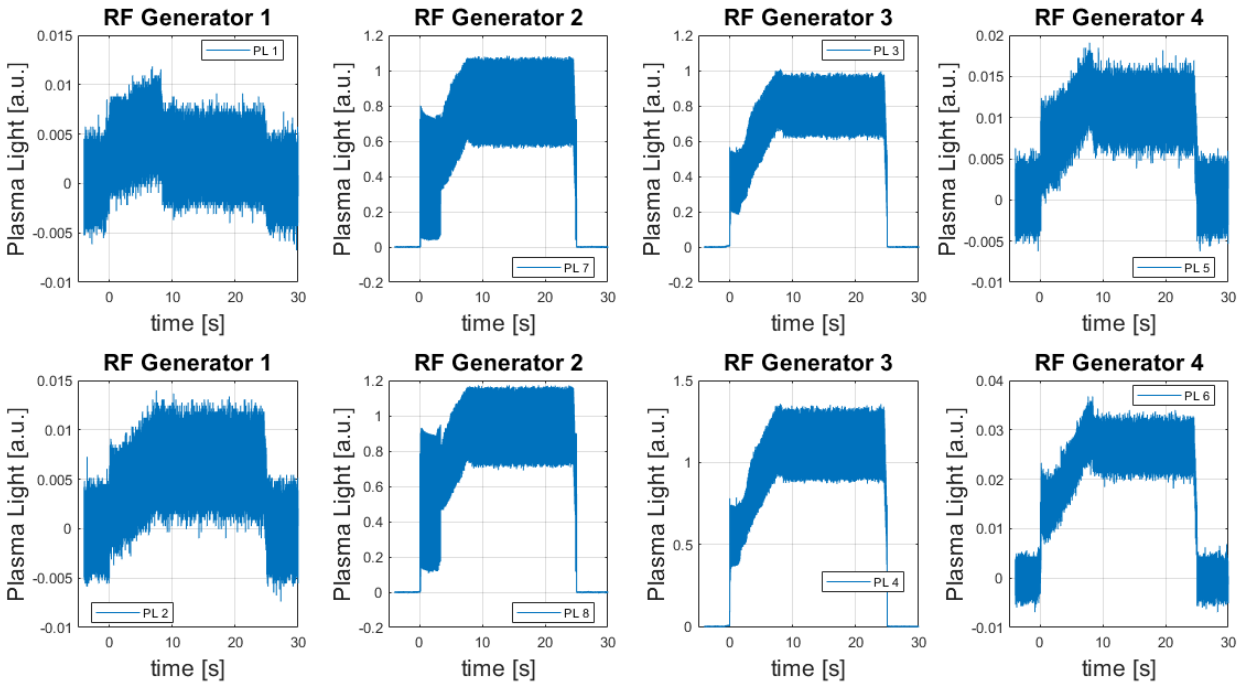

Figure 5.1: Plasma light signal while RF generator 2 and 3 were ON

The experimental operations with different experimental setup permitted to understand, to study and to evaluate the response of system and the relations between the plasma light intensity and the parameters for the ignition.

Figure 5.2 present a RF power scan at fixed ignition parameter PG current and ion-source's pressure (i.e. fixed inlet pressure).

Figure 5.2: Scan of RF Power

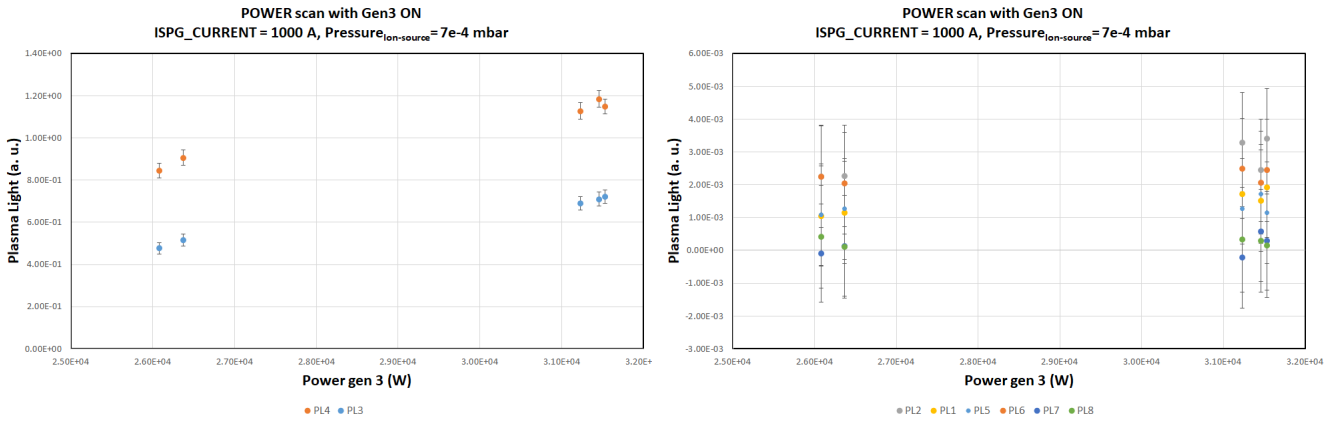

(a) Plasma lights in the segment of the generator 3 (ON) (b) Plasma lights in the others segments

The plasma light in the segments of the generators on present an intensity that linearly increase with respect of RF power of the generators in question. The others plasma lights present just a noise signal, this can mean that the plasma is concentrated just in the drivers corresponding to the generators on and the light it emits is not enough to disturb the other plasma lights.
Particularly noticeable is that even the plasma lights in the same segment do not catch the same light intensity even if the data is taken at the same time and in the same operating conditions, this can be due to a different offset of the plasma light or to a different operation of the RF coils in the drivers.

Figure 5.3 present a PG current scan for fixed ignition ion-source's pressure and RF power.

Figure 5.3: Scan of PG current with one RF generator on

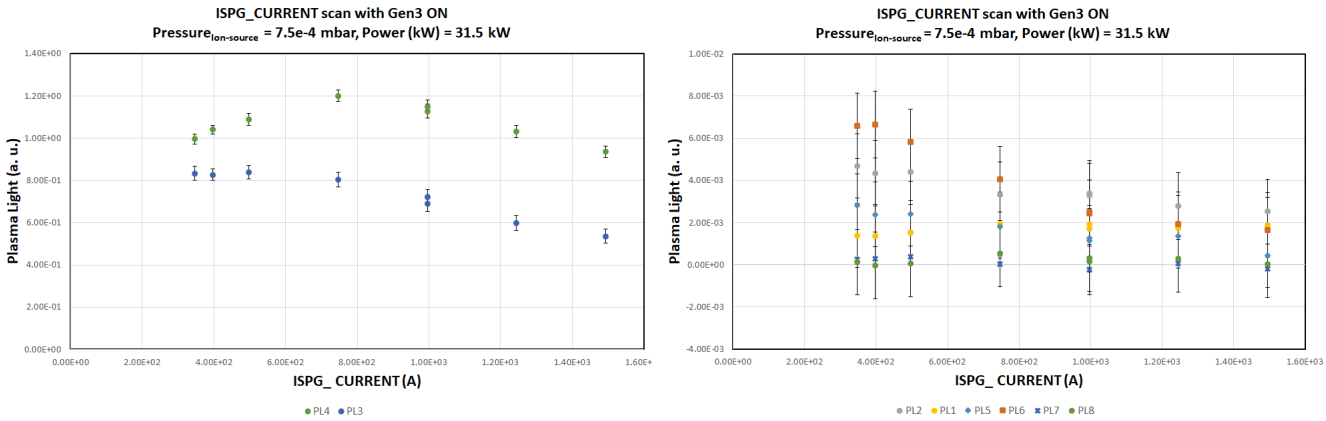

(a) Plasma lights in the segment of the generator 3 (ON) (b) Plasma lights in the others segments

From the figure is possible to see that the intensity difference between two plasma light on the segment of generator 3, strongly depend on the PG current, in particular at low current the intensity gap between the two is around $\Delta A_{3-4} = 2$ a.u. but increases and stabilize around $\Delta A_{3-4} = 4$ a.u. from $I_{PG} = 800$ A on.

Figure 5.4: Scan of PG current with 2 RF generators on

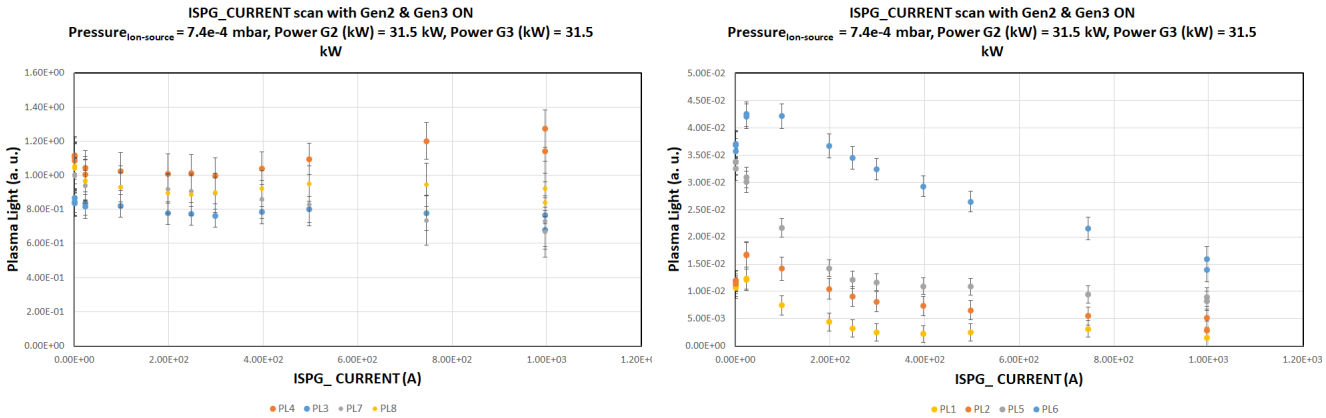

(a) Plasma lights in the segment of the generators 2 and 3 (ON) (b) Plasma lights in the others segments

From figure 5.4 what can be seen is that two generator, for example 2 ad 3, have plasma lights behaving differently on to the other but also the intensity gas difference of the plasma light of the same generator differ from the ones of the other. As it was said before, for generator 3 the gap difference begin around $\Delta A_{3-4} = 2$ a.u. and stabilize at $\Delta A_{3-4} = 4$ a.u. from $I_{PG} = 800$ A on; for generator 2 the gap difference at $I_{PG} \sim 0$ A is almost zero but increase with increasing the PG current until it stabilize around $\Delta A_{3-4} = 2$ a.u..

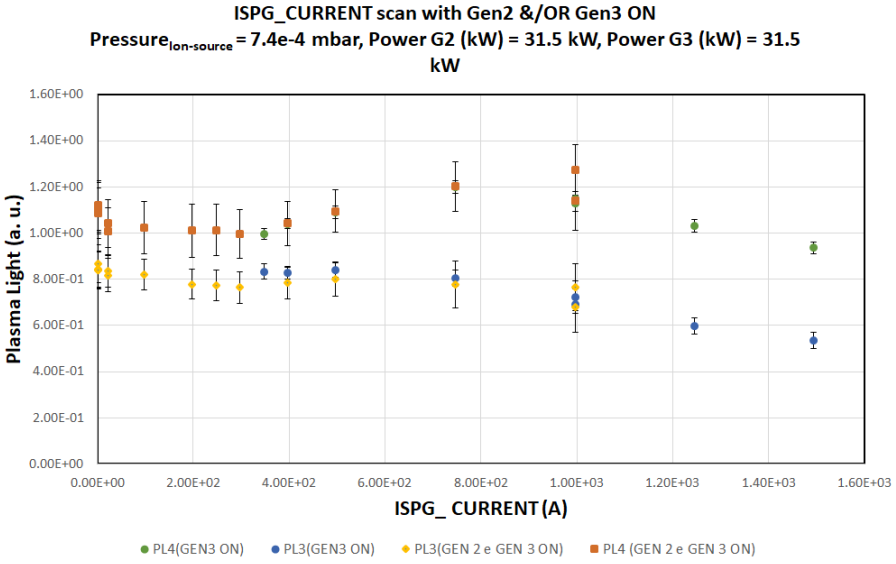

Figure 5.5: Comparison of the two PG current scans

The presence of one generator or more generators on does not seem to disturb the plasma lights signal even at different I_{PG} and with the same RF power.

Figure 5.6 present a ion-source's pressure scan at fixed ignition PG current and two different RF power of the generator 3.

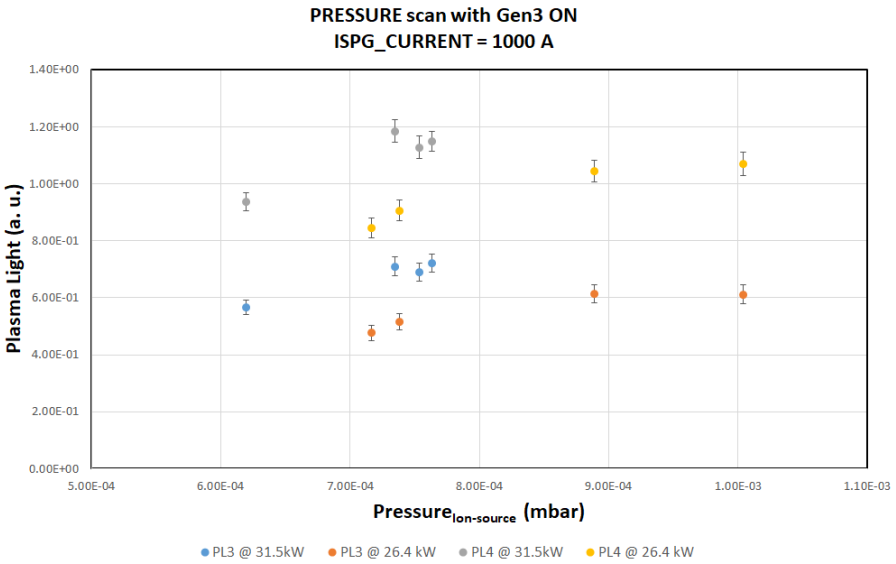

Figure 5.6: Scan of the ion-source's pressure

5.2 Filament as a probe

Langmuir probes to investigate the plasma density are not available for this first campaign of SPIDER operation. Hence the only way to find an estimated value is to use the spectroscopy, but this is outside the scope of the present thesis work. However, in the first operation of characterization of plasma, there has been five shots in which the filaments behaved like a Langmuir probe.

A conductive electrode, inserted in a discharge and biased positively or negatively to draw electron or ion current, is one of the earliest and still one of the most useful tools for diagnosing a plasma. These probes, introduced by Langmuir, are usually called Langmuir probes. Probes are usually quite small and under suitable conditions, produce only minor local perturbations of the plasma.

The voltage and current of a probe lead to a typical probe voltage–current characteristic like in figure 5.7. The probe is biased to a voltage V_B with respect to ground (in the case of SPIDER filaments V_B was fixed at -60 V) and the plasma is at a potential Φ_P with respect to ground. At the probe voltage $V_B = \Phi_P$, the probe is at the same potential as the plasma and draws mainly current from the more mobile electrons, which is designated as positive current flowing from the probe into the plasma. For increasing V_B above this value, the current tends to saturate at the electron saturation current, but, depending on the probe geometry, can increase due to increasing effective collection area. For $V_B < \Phi_P$, electrons are repelled according to the Boltzmann relation, until at Φ_f, known as the floating potential, the probe is sufficiently negative with respect to the plasma that the electron and ion currents are equal such that $I = 0$. When further reducing the voltage, the current is increasingly ion current (negative into the plasma), tending to an ion saturation current that may also vary with voltage due to a change of the effective collection area. The magnitude of the ion saturation current is much smaller than the electron saturation current due to the much greater ion mass.

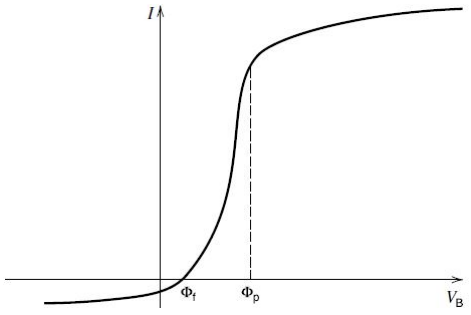

Figure 5.7: Typical $I - V_B$ characteristic for a Langmuir probe

In order to minimally disturb the plasma and also for ease of construction, Langmuir probes are often thin wires with the wire radius $r < \lambda_{De} = \frac{\varepsilon_0 T}{q\, n}$ (Debye length is a measure of a charge carrier's net electrostatic effect in solution and how far its electrostatic effect persists).
Consider the tungsten filament in use, the physical probe area $A \ll s^2$, where s is the sheath thickness, such that the collecting area A is essentially independent of s. As said previously, if a large voltage is applied to the probe, then $s \ll \lambda_{De}$, and A is large enough to satisfy the above condition. For this reason we expect that the probe won't strongly perturb the plasma. We can consider the probe sufficiently negatively biased to collect only ion current. The collected current by the probe is

$$I = -I_i = -e\, n\, u_B\, A \tag{5.1}$$

where c_s is the ion-sonic velocity is given by

$$c_s = \left(\frac{eT_e}{m_i}\right)^{1/2} \tag{5.2}$$

If T_e is known, then the density at the sheath edge n is determined from the measurement of I.

From the experimental shots and in the approximation that the plasma ions are mostly H^+, it was possible to obtain the density n using the previous relationships using for the electrons temperature $T_e = 10$ eV. It was also possible, to relate the density with the RF power of the generators in the Drivers with the filaments on.

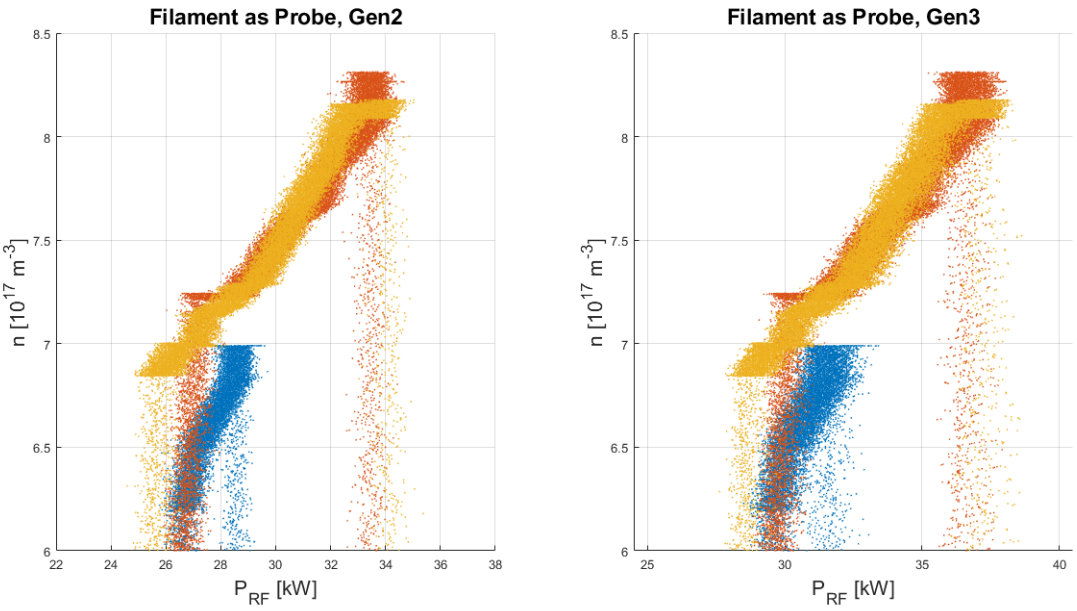

Figure 5.8: Relation between Plasma density and RF Power

As it can be seen form figure 5.8 the two generators with the filament present a similar behavior, in the linear part corresponding to the moment in which the filament current present a stable behavior. In particular in this region can be found a linear relation between the RF power and the density given by a fitting formula like $y = a + b \cdot x$ with parameters:

Valve	Coefficient	Value	R^2
Generator 2	a	1.0174	0.8552
	b	0.2144	0.8552
Generator 3	a	0.6808	0.8588
	b	0.2037	0.8588

The two generators present just a slight difference that can derive from an different initial offset.

5.3 Plasma density Model

The main aim of this section is to build a one-dimensional model of the plasma in the path PG-drivers in order to obtain the density profile along the path. In the end of the section is than presented an improvement of the model that consider also the magnetic filter field and the cylindrical shape of the drivers.

The model is based on two main equation, the stationary equation of motion and the continuity equation both evaluated under some assumptions.
To model the plasma in the driver region is considered a plasma with only an ion species, H_2^+, in the case of a H_2 plasma: considering just one ion specie is generally not true for a molecular gas, but this simplify the problem and does not result in too large an approximation error. The gas temperature is considered as external parameter, in particular, taken as $T_{H_2} = 600$ K; the ion temperature is taken equal to the neutral gas temperature, $T_i = T_{H_2}$.
The firsts equations taken into account are the stationary equation of motion for the two species, electrons and ions

$$\begin{aligned} 0 &= -n_e e(\vec{E} + \vec{u_e} \times \vec{B}) - \nabla p_e - m_e n_e \nu_{ei}(\vec{u_e} - \vec{u_i}) - m_e n_e \nu_{en} \vec{u_e} \\ 0 &= +n_i e(\vec{E} + \vec{u_i} \times \vec{B}) - \nabla p_i - m_i n_i \nu_{ie}(\vec{u_i} - \vec{u_e}) - m_i n_i \nu_{in} \vec{u_i} \end{aligned} \tag{5.3}$$

where ν_{ei}, ν_{ie}, ν_{en}, ν_{in} are the momentum transfer collision frequencies between electrons, ions and neutrals. In the first analysis the magnetic field can be neglected with respect to the other terms and since the plasma is made of only one ion specie, the electron density and the ion density are equal ($n_e = n_i = n$). With these approximation and considering the ions- electrons elastic collision with $n_e m_e \nu_{ei} = n_i m_i \nu_{ie}$, the equations 5.3 leads to:

$$\begin{aligned} 0 &= -ne\vec{E} - \nabla p_e - m_e n \nu_{ei}(\vec{u_e} - \vec{u_i}) - m_e n \nu_{en} \vec{u_e} \\ 0 &= +ne\vec{E} - \nabla p_i - m_e n \nu_{ei}(\vec{u_i} - \vec{u_e}) - m_i n \nu_{in} \vec{u_i} \end{aligned} \tag{5.4}$$

Now, being the temperature gradient negligible with respect to the density gradient, $\nabla_p = k_B T \nabla n$, adding the equations 5.4 results:

$$0 = -k_B(T_e + T_i)\nabla n - (m_e \nu_{en} + m_i \nu_{in})\Gamma \tag{5.5}$$

where the ambipolar flux is assumed as $\Gamma = n\vec{u_e} = n\vec{u_i}$. The equation 5.5 can be rewritten as

$$\Gamma = -D_a \nabla n \tag{5.6}$$

where D_a is the ambipolar diffusion coefficient

$$D_a = \frac{\mu_i \, D_e + \mu_e \, D_i}{\mu_i + \mu_e} \tag{5.7}$$

and

$$\begin{aligned} D &= \frac{k_B T}{m\nu} \quad \text{Diffusion Coefficient} \\ \mu &= \frac{q}{m\nu} \quad \text{Mobility Coefficient} \end{aligned} \tag{5.8}$$

The momentum transfer is given by $\nu_{ab} = n_a n_b K_{ab}$ where K is the rate coefficient of the collision in question that can be found tabulated and depends on the temperature of the specie. The total momentum transfer for electrons is the sum of the momentum transfer of the collision electrons-electrons, electrons-ions, electron-neutral, electrons-neutral (the same for ions).
The continuity equation for electrons reads:

$$\nabla \cdot \Gamma = G - L \tag{5.9}$$

where G is the source term i.e. $G = n_{gas} \; n \; K_{eH2}$ and K_{eH2} is the rate coefficient for electrons H_2 ionizing collisions while L is the loss term due to recombination given by $L = n \; n \; K_n$ and K_n the recombination rate

coefficient.
Combining than equation 5.6 and 5.9 leads to the model equation:

$$\nabla \cdot (-D_a \nabla n) = G - L \tag{5.10}$$

in this way, the boundary condition at the PG and at the end of the Drivers is the Bohm condition:

$$(-D_a \nabla n) = 0.6\, n\, c_s \tag{5.11}$$

with $c_s = (q\, T_e/m_i)^{1/2}$ the ion-sonic velocity.
The electron temperature is taken with a distribution shown in figure 5.9, in particular is 2 eV at the PG and 10 eV in the Driver. To notice is that also the temperature profile is a model, in the situation without magnetic field is very difficult to have such a profile and also to be able to reach the 10 eV in the drivers while having 2 eV at the PG.

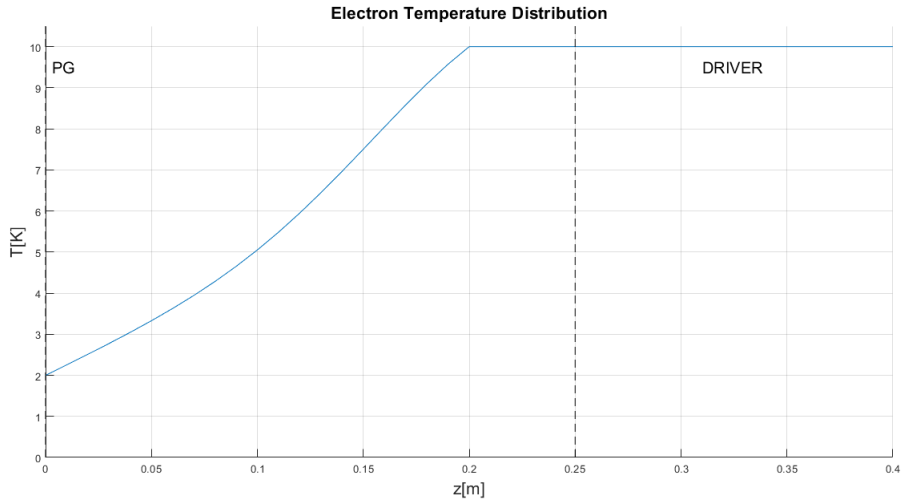

Figure 5.9: Electron temperature distribution

5.3.1 Magnetic Field

In the SPIDER experiment is installed a transverse magnetic field inside the negative ion source and accelerator, called magnetic filter. The motivations for building a transverse magnetic field are essentially:

- guaranteeing beam efficiency by introducing in the ion-source a filter field on the upstream side of the Plasma Grid (PG) to reduce the average energy and density of electrons approaching the grid and for optimizing the extraction of the negative ions.
- limit the heat loads caused by electrons and also achieving the required ion beam optics by introducing in the accelerator a local suppression field on the downstream side of the PG to eliminate the co-extracted electrons. As this field marginally penetrates in the plasma source upstream of the PG, it also enhances the extraction of negative ions and reduces the co-extracted electrons. As in most existing experiments, the Suppression Field is generated by arrays of permanent magnets embedded in the EG and has two opposite peaks along each beamlet, in order to reduce the resulting deflection of the ions.

The SPIDER Filter Field has been designed to be uniform and confined within the Ion Source volume.
The SPIDER PG busbar-system includes two lateral bars on the sides of the PG and three PG ”return” bars placed on the back side of the Ion Source in between the RF Drivers, with upper and lower connections constituting a solenoid-like path for the PG current. The system produces a fairly uniform Filter Field on the upstream side of the PG (~ 4.5 mT) and a much smaller field in the Accelerator (< 0.5 mT) and in the RF drivers (< 1.0 mT) (As shown in figure 5.10) with a current of 2.4 kA .

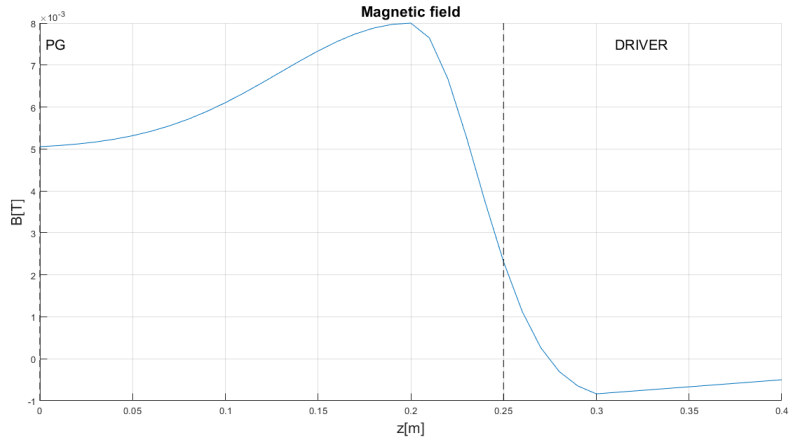

Figure 5.10: Profile of transverse horizontal field B_x generated by current flowing in Plasma Grid along the RF drivers and related busbar system

A transverse magnetic field is necessary inside a negative ion accelerator for deflecting as early as possible the co-extracted electrons and those generated by stripping reactions with the background gas.
For this purpose, arrays of permanent magnets are in use and embedded in the EG, they are arranged in horizontal arrays above and below the apertures. The arrays are magnetized along the beam direction with alternate orientation, so that two symmetrical peaks of transverse field having opposite orientation are produced along each beamlet. The profile of the local electron Suppression Field By in SPIDER is shown in figure 5.11.

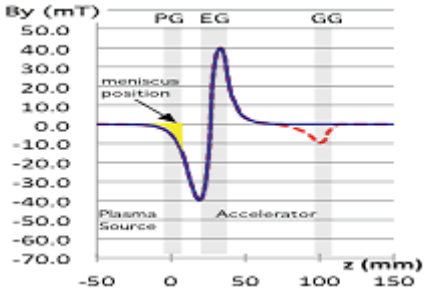

Figure 5.11: Profile of the transverse vertical field B_y produced by electron suppression magnets embedded in the accelerator grids of SPIDER

The implementation of the magnetic field in the model imply that in the equation of motion 5.3 the term with the magnetic field is no more negligible and the diffusion coefficient that become dependent on the strength of the magnetic field as:

$$\mu_\perp = \frac{\mu}{1+\left(\omega_c/\nu\right)^2} \qquad D_\perp = \frac{D}{1+\left(\omega_c/\nu\right)^2} \tag{5.12}$$

with $\omega_c = qB/m$ the gyration frequency.
The boundary condition used at the PG and at the Driver, now differs by a factor, involving the existence of a magnetic multipole confinement which structure of the magnetic field just is discussed and it is a periodic arrangement of magnetic rows in a rectangular geometry. A useful parameter in confinement is the fraction f_{loss} of diffusing electron-ion pairs that will be lost at the wall, in this case, at the PG. The boundary condition at the wall, PG, for the ambipolar diffusion of plasma within the field-free discharge volume is then

$$\Gamma_{PG} = f_{loss}\, n\, c_s \tag{5.13}$$

with $c_s = (q\ T_e/m_i)^{1/2}$ the ion-sonic velocity. At the Driver, as boundary condition is used the Bohm criteria

$$\Gamma_{Driver} = 0.6\ n\ c_s \tag{5.14}$$

The model density distribution along the path PG-Driver in the two situation i.e. with or without the magnetic filter, results:

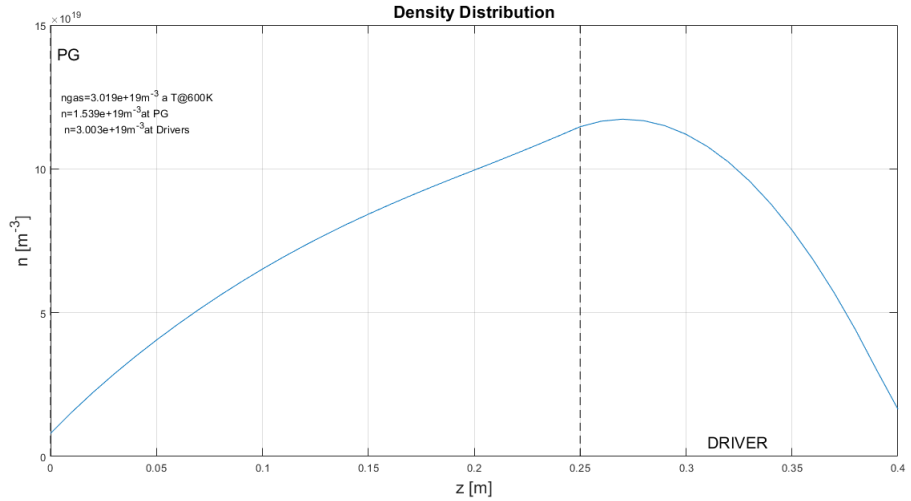

Figure 5.12: Density distribution without $\vec{B}$

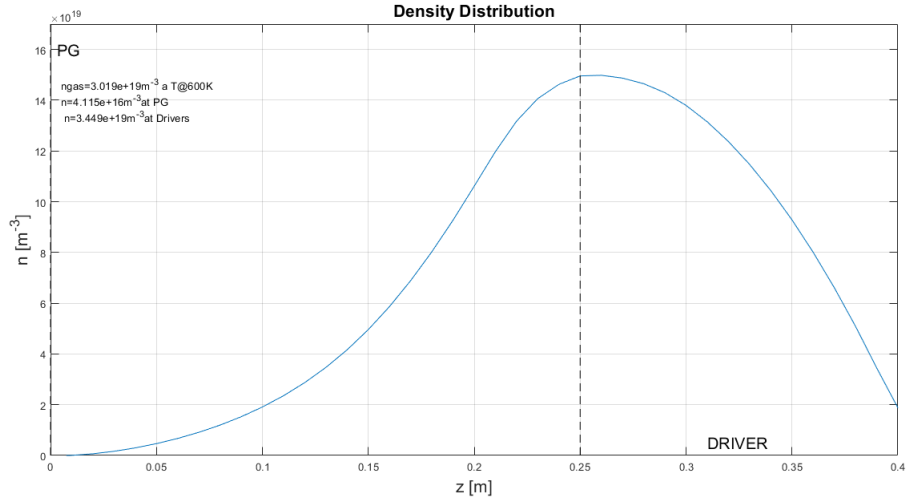

Figure 5.13: Density distribution with $\vec{B}$

As it is possible to see from figure 5.12 and 5.13 the magnetic filter field increase, move and change the distribution towards the driver region.

An improvement of the model can come from the consideration of the cylindrical shape of the Drivers and considering the obtained density at the driver as the one in the center of the cylinder.
In order to obtain the radial profile of the density in the driver it is necessary to solve the diffusion equation in azimuthal symmetric coordinates:

$$\frac{d^2n}{dr^2} + \frac{1}{r}\frac{dn}{dr} + \frac{G}{D} = 0 \tag{5.15}$$

At very low pressure and in the driver it is possible to use an approximate solution called ”free-fall solution” which uses a collisionless assumption. The collisionless absumption is usually wrong for the drivers, but not affected by a big error if the collisions are considered concentrate in the central node, i.e. along the axis, from which I solve the model.
For diffusion in a infinitely long cylinder of radius R (driver radius $R = 15$ cm) was obtained (Godyac, 1986):

$$\frac{n(R)}{n(0)} \simeq 0.8\left(4+\frac{R}{\lambda_i}\right)^{-1/2} \tag{5.16}$$

The resulting solution for the normalized density and the density along the driver azimuthal direction is shown in the following figure:

Figure 5.14: Driver azimuthal density

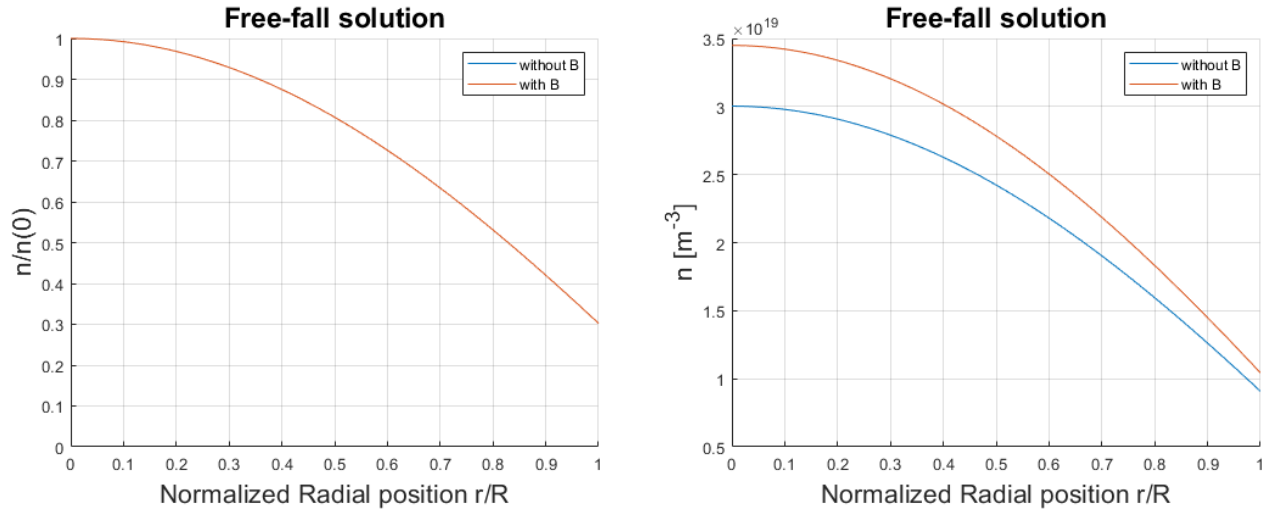

(a) Normalized density

(b) Density

Chapter 6

Conclusions

As it was said in the introduction, the aim of the SPIDER experiment is to study and to test the RF ion source for ITER. The aim of the first operation has been to study the system and to reach a satisfactory plasma ignition in order to go further on with the full operation of the experiment.

The analysis of the GVS permitted to find out the different behavior of the two micrometric valves i.e. the choke of the valve VC3002, the relation between the pressures in the system and so to forecast the behavior even with only one pressure gauge available. Moreover, the development of the LTSPICE model permits now to study a thought setup and to see the outcome.

The filament analysis has been necessary to evaluate the emitted current and the limited space charge and with it, to find a suitable adjustment in order to prevent the filaments to overheat and ruin.

The first ignition have been the first step for further studies, in particular the study of one of the criticism met: the discharge in the rear side of the drivers permitted to find a solution to reduce the probability of this type of discharge; in the past few days an additional shielding in the rear side of the drivers has been put in place.

As it was underline in the text, the spectroscopy was out of the context but its results can be used with the ones obtained in the last chapter as comparison or confirm of the different approaches.

In the future the plasma density model developed could be improved and extended to higher dimension and compared with other experiment results.

In conclusion, the models developed in this thesis and the analysis of the system will be helpful in guiding the future experimental activity and SPIDER with the perspective of a better understanding of the physics involved in the ITER project.

Appendix A

LTSPICE

The LTSPICE model built for the SPIDER gas injection system is based on the measure made with the open vessel of the pipes dimension, the knee angles and the valves involved. The model can be divided in 3 major parts: the injection line, the drivers pipelines and the measure line.
The nominal resistances are calculated based on the diameter of the pipe and in unit of length like the capacity. The choice of dividing the pipeline system have two main reasons: the first one is purely ”figurative” i.e. it is divided into straight and angular parts exactly as in the SPIDER experiment, the second one is more physic, in order to improve the accuracy of the model is better if the program can work trough more elements because it works with differential equations. All the formulas used for the calculation have been presented in section 2.3 taking into account that the gas flowing through the pipes is hydrogen.

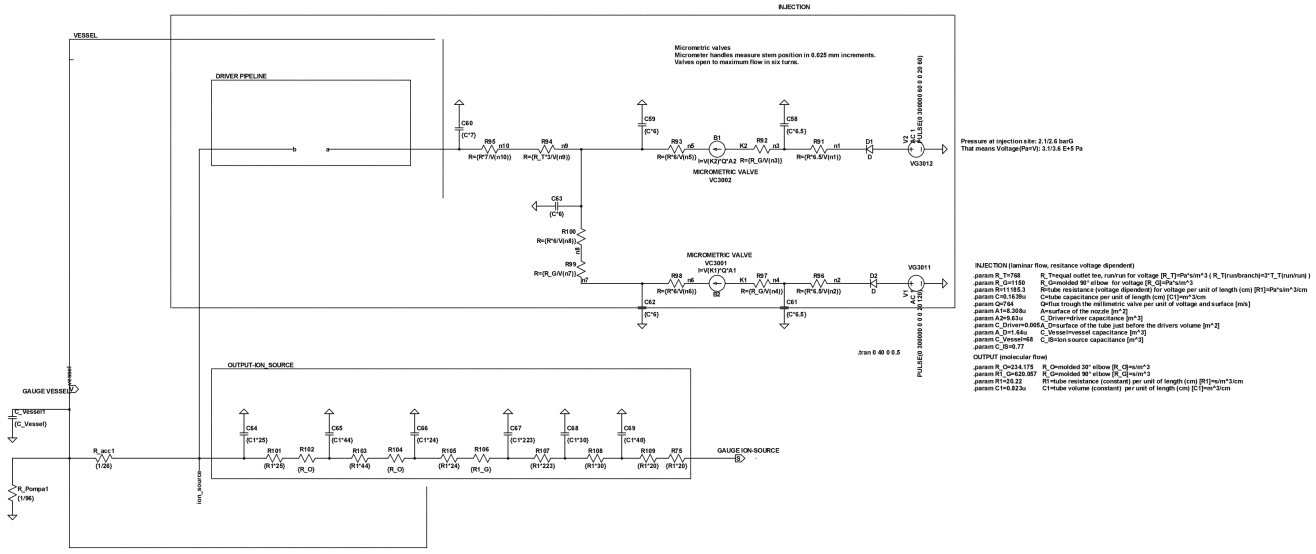

Figure A.1: Overall view of the LTSPICE model

The injection line (figure A.2(a)) is characterized by the two DC generators analogs to the mechanical valves ON/OFF VG001 and VG002 and the two dependent current generators representing the chocked flow of the micrometric valves VC3001 and VC3002. The peculiarity of these two last generator lays in the fact that their flow is the product of three parameter, one fixed: Q , the flux per unit of surface and unit of voltage depending only on the geometry of the pipe; A the cross sectional area of the flow constriction that has been calibrated with the micrometric valve ticks as presented in section 2.4.1; V the voltage flowing through the controlled generator depending on the initial voltage setup. In particular the injection line is characterized by pipes with a diameter of 4.570 mm.
The measure line (figure A.2(b)) is mainly characterized by the presence of the two gauges the one in vessel

and the one at the output of the ion-source. The line of the vessel gauge present only two electrical element with fixed value: resistors accounting for the accelerators grid and for the cryopumps and a capacitor with a very high capacity representing the volume vessel. The line of the ion-source gauge have the same characteristic of the injection line but the pipe here has a diameter of 10.22mm.

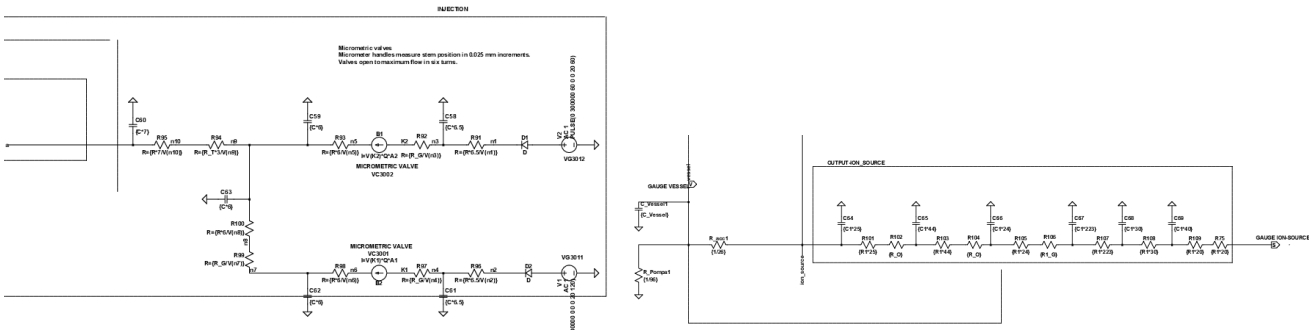

(a) Injection (b) Measure

Figure A.2: LTSPICE model

The line that connects the injection and the measure line is the drivers piping system (figure A.3). It has the same pipe-size of the injection line but present other eight dependent current generators representing the flow from the small pipeline to the volume of the drivers (810 dm^3), in this case, the cross sectional area of the constriction is fixed as the area of the injection pipeline.

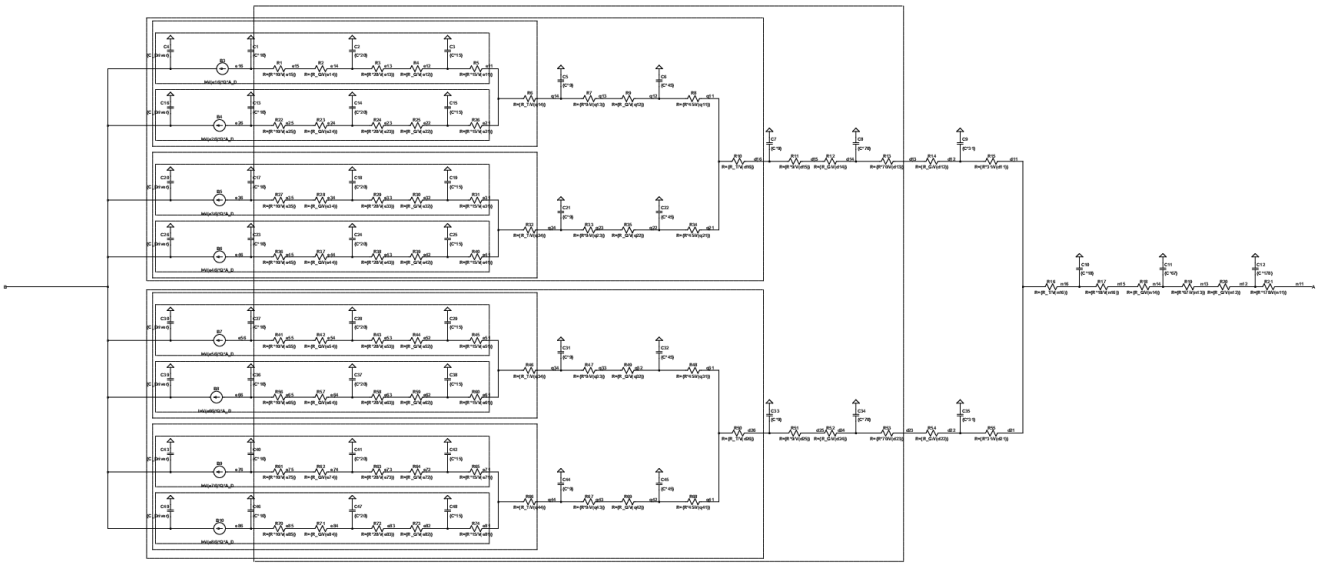

Figure A.3: LTSPICE model of the Drivers region

Bibliography

[1] D. Marcuzzi, P. Agostinetti, M. Dalla Palma, F. Degli Agostini, M. Pavei, A. Rizzolo, M. Tollin, L. Trevisa, et al., Detail design of the beam source for the SPIDER experiment, in: Fusion Engineering and Design 85 (2010) 1792–1797

[2] P. Agostinetti, V. Antoni, M. Cavenago, G. Chitarin, N. Marconato, D. Marcuzzi, N. Pilan, G. Serianni, P. Sonato, P. Veltri and P. Zaccaria, et al., Physics and engineering design of the accelerator and electron dump for SPIDER, in: Nucl. Fusion 51 (2011) 063004 (16pp)

[3] Irving Langmuir and Katharine B. Biodgett in: Currents limited by space charge between coaxial cylinders

[4] Michael A. Lieberman and Allan J. Lichtenberg, in: Principles of Plasma Discharges and Materials Processing, Second Edition 2005, WILEY

[5] P. Veltri, E. Sartori, M. Cavenago, G. Serianni, M. Barbisan, and B. Zaniol, et al., Study of electron transport across the magnetic filter of NIO1 negative ion source, in: AIP Conference Proceedings 2017 1869:1

[6] V Toigo et al., The PRIMA Test Facility: SPIDER and MITICA test-beds for ITER neutral beam injectors, in: 2017 New J. Phys. 19 085004

[7] E. Sartori, Simulation of the gas density distribution in the large vacuum domain of SPIDER, 23/12/2014

[8] ITER Organization, https://www.iter.org/

[9] Pjush Kundu, Ira Cohen and David Dowing, in: Fluid Mechanics

[10] A. Guggenheim, in: Termodinamica, 1952

[11] C. Kittel, in: Introduzione alla Fisica dello Stato Solido, 2008